University of Twente

Bachelor thesis

Sustainable process technology group

Kinetic modelling of LDPE hydrogenolysis using non-linear regression

Author
T.K.H. van der Lee

t.k.h.vanderlee@student.utwente.nl
s2382040

Academic years 2019 - 2023

Daily supervisor
IR. E. van Daatselaar
Faculty of Science and Technology (TNW),
Sustainable Process Technology (SPT)

Head supervisor
DR. M.P. Ruiz Ramiro
Faculty of Science and Technology (TNW),
Sustainable Process Technology (SPT)

July 10, 2023

Abstract

The issue of plastic pollution has escalated in recent decades, with no clear solution for recycling it into usable high-quality materials. One possible method to address this is a low-temperature chemical process called hydrogenolysis which can break down polyolefins into valuable resources such as naphtha. However, there has been limited research on the kinetic modelling of this process, which could potentially offer deeper insights into the chemical and physical occurrences. The reaction process involves a gas phase, initially comprising solely of hydrogen, and a liquid phase with a catalyst, where the hydrocarbons crack into smaller components. This thesis researches how the experimental results can be predicted by a kinetic model when using non-linear regression in Matlab and assuming Knudsen diffusion. The results from the model will be compared to the provided experimental results from the SPT group of the University of Twente. This process will use LDPE feedstock and a porous 5wt% Ru/C catalyst. The purpose of this thesis is to offer more detailed insight into the experimental outcomes and the processes occurring within the reactor. The objective of the research is to attain a model that can accurately forecast the yield, pressure, and residual hydrogen from the experimental results. The model will predict mass transport between the gas and liquid phase, internal resistances of the catalyst, and factors such as the dependence on the hydrogen concentration, changing density and volumes, and the compressibility of the gas phase. The results indicate that the model has a good ability to predict experimental outcomes, with only a few exceptions. After analysing the results, it can be inferred that the yield obtained from the experimental measurements may not be entirely precise and could be higher for certain smaller compounds. The evaporation of hydrogen is also likely not coupled with the evaporation of the hydrocarbons based on the liquid diffusion ratio. Finally, it is not possible to describe the effectiveness of the catalyst solely through Knudsen diffusion. More information about the catalyst characteristics is also needed. These findings hold significant importance as they offer precise suggestions for improving both the experimental measurements and the modelling of the chemical process.

Contents

Acknowledgements

The author would like to thank IR. E. van Daatselaar with providing weekly assistance during the bachelor assignment and helping with general questions, feedback, LaTeX help, Aspen+ modelling, and reviewing the paper. E. van Daatselaar also supplied a basic model which had a similar cracking mechanism based on the work of Marathe et al. (2019a, 2019b) and the experimental data using the SPT experimental setup of the University of Twente.
The author would also like to thank J.A. Wood for helping with connecting the ordinary differential equation to the regression system and making it fit against the experimental data.
The author is obliged to PROF.DR.IR. D.W.F. Brilman for providing the reader of the Advanced chemical reaction engineering course which was used for the mass transport processes.
Finally, the author would like to thank IR. T.N. van Schagen for helping with describing the kinetic rate constants as a function based on the respective carbon length. This work could not be completed within the available time for this thesis.

Chapter 1

Introduction

Plastic pollution has been an environmental issue for decades. Due to their excellent properties like strength, flexibility, and durability, we have been using more and more plastic for decades as packaging materials or for other uses of convenience. But these amazing properties have also meant that they create an enormous ecological problem: plastics barely break down naturally. This has caused plastics to accumulate in the environment [1], harming all kinds of life in the process. Because plastic is so hard to break down, it is dumped in landfills [2], shipped to third-world countries to be dealt with, or incinerated, releasing it as carbon dioxide into the atmosphere. In addition, plastics are currently made from fossil fuels which is an unsustainable resource.

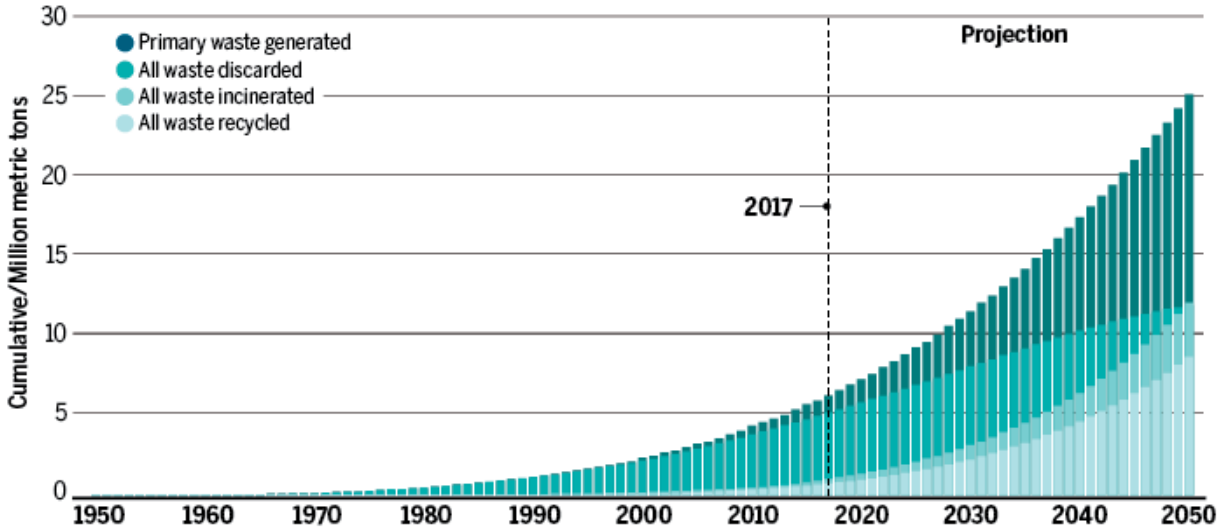

Figure 1.1: Global plastic waste management until 2017 [3]

Currently, only 9% [4] globally of all plastic produced is recycled as of 2022. The European Union is well above the global average with 38% recycled in 2020 [5]. This is done by sorting plastics by type and mechanically recycling them into plastics that can be reused by heating and reforming them. The problem is that not all plastics can be recycled this way. Plastics are difficult to recycle mechanically due to mixed polymers [6], contaminants, dyes, and general polymer degradation during recycling. This is why a better way of recycling is necessary. One promising way is to recycle chemically instead of mechanically, see figure 1.2. Examples of chemical recycling are: hydrocracking in the presence of hydrogen gas in a thermal cracker, gasification, and hydrogenolytic catalytic cracking to create smaller carbon chains. While the thermal cracker uses temperatures around 550–1150 Kelvin [8], using a lot of energy in the process, hydrogenolysis can be done as low as 440 Kelvin according to some reports [9, 10]. The process described in this report is a hydrogenolysic catalytic reaction, which means that the polyolefins crack on the catalyst surface in the presence of hydrogen.

Hydrogenation catalytic cracking is a new technique that could recycle plastics into a naphtha product stream which could then be used for producing new plastics. This implies that recycled plastics do not have a degradation in quality, as with other recycling methods, and have a lower carbon footprint. The technique can be applied to multiple types of polyolefins such as polyethylene and polypropylene, which are made of simple olefins. It can be used to close the carbon cycle, by feeding the product into a steam cracker. This means that no new fossil fuels will need to be used to produce plastics, making it a sustainable process.

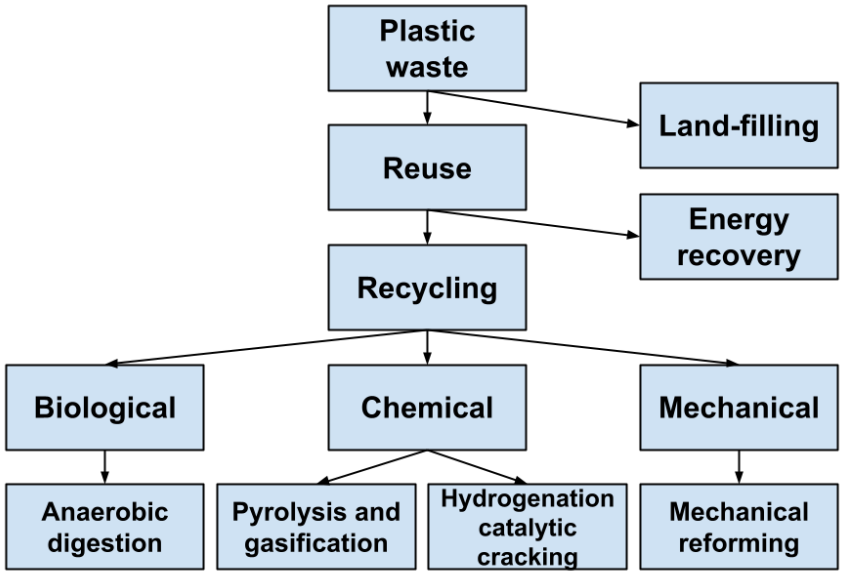

Figure 1.2: Plastic recycling techniques map (modified) [7]

Even though the process shows potential, there are still a lot of problems such as high energy demand compared to fossil fuels, the cost and reuse of the catalyst, and different reaction mechanisms for different plastics [8]. Current research into the hydrogenolysis of plastics has mostly been done experimentally due to the complex nature of diverse hydrocarbon interactions. The research has been focused on determining the best reaction parameters for optimal product results such as catalyst choice, hydrogen pressure, temperature, agitation rate, and reaction time. One of the current findings for the catalyst is that porous platinum or ruthenium gives the best reaction speed and selectivity [9, 10, 11, 12, 13, 14]. The other reaction conditions can range quite a bit. For instance, the temperature can range from 440 to 700 K [8, 9, 14] and the hydrogen pressure can range from 20 to 180 bars.

The desired end product is a liquid naphtha stream because of its economic value and the ability to turn it back into monomers which can be used again to make high-quality plastic. In addition to experimental research, there has also been a limited amount of modelling of the reaction by taking the experimental data and applying this to a kinetic model to learn more about the process and how it can be optimised [9]. In this report, a kinetic model of the experimental set-up, as used within the SPT group of the University of Twente, will be modelled.

Chapter 2

Research goal

The focus of this research is to develop a kinetic model that can predict the results of the experimental hydrogenolysis of plastic. The research will also answer which parameters can be determined or assumed in order to make the model more accurate. The purpose of this is to gain a deeper understanding of the chemical processes that occur within the reactor, which cannot be measured through direct experimentation. This information can help identify which reaction parameters have the most significant impact on the yield distribution of the final product. The researched parameters include mass transport limitations between multiple phases, catalyst selectivity, hydrogen influence on the reaction rate, density, and compressibility.

The research plan is to attain a model by determining the kinetic reactions between different alkanes and calculating the parameters, like reaction and mass transfer rates, by using non-linear regression with the provided experimental results using Matlab software. The experimental data was supplied by IR. E. van Daatselaar who is a PhD student in the Sustainable Process Technology group of the University of Twente and who is the daily supervisor in this bachelor thesis. The kinetic model can be assumed to be improved if it can accurately predict the experimental results of product weight distribution, pressure and amount of hydrogen used. Regression analyses such as comparing the data to the results, residual probability, analysis of variance, and correlation of parameters will be done to test the validity of the model against the experimental results.

The model will be made based on the work of various state-of-the-art research papers which have similar research objectives [9, 10, 14, 15, 16], of which some will be used for close comparison. The model is also based on the material that is taught in the chemical science and engineering bachelor of the University of Twente such as the mass and heat transfer classes, kinetics and catalysis and introduction to chemical reaction engineering. Some material which is given in the master course such as advanced chemical reaction engineering and modelling in Aspen+ will also be used to some extent.

In this report, the theory is explained first, which is the mathematical basis for the model. After this, more information on the experimental conditions and model method is provided which includes the made assumptions. This is followed by the results and discussion including the validation of the model against the existing literature. Finally, the conclusion is given and some ideas for future improvements.

Chapter 3

Theory

3.1 Background information

Plastic recycling is the process of making new plastic from old plastic. There are many ways in which plastic can be recycled, ranging from anaerobic digestion to mechanical reforming, as can be seen in figure 1.2. The main challenges towards general recycling are cost, quality and complexity [2, 4, 6, 7].

Cost is a challenge because recycling is a difficult and often energy-intensive process which is usually more expensive than making plastics from fossil fuels [2, 6, 7].

The quality of the recycled material depends on the method of recycling. If the plastic is broken down into the monomers from which it was formed, then the plastic can be made brand-new again. However, some types of recycling like mechanical recycling, which is the process of grinding [17], washing, and compounding the plastic, lower the quality of the plastic by so much that it effectively can not be repeatedly recycled without large losses in quality [6]. This method will therefore on its own never be able to recycle plastic effectively.

Lastly, there is the problem of complexity. Plastic is often layered into other materials, consists of several types of plastic, is not separated correctly by people, is contaminated with other materials or has additives like binders, fillers, dyes or plasticizers [6, 7]. These contaminations make the recycling process even more difficult since the desired result would be pure plastic with a specific property, and therefore can often not be a mixture of different plastics.

Because of the challenges mentioned above, most of the plastic today is dumped in landfills [6, 7], ends up in the environment or is used as an energy recovery technique to produce energy, releasing a large amount of carbon dioxide into the environment by burning the plastic waste. That is the research problem in this thesis which it intends to improve. The only type of recycling that is used currently on a larger scale is mechanical recycling [6, 7, 13], which unfortunately often reduces the quality of the plastic significantly or is only viable for specific types of plastic.

However, hydrogenolysis of polyolefins shows great potential compared to other types of recycling techniques. It is less energy-intensive [9] than a lot of other techniques because the catalyst allows reaction at lower temperatures as low as 440 Kelvin. This is beneficial for operating costs and the environment. It can also have specific selectivity towards certain desired end products and has a relatively high rate of reaction [9, 12]. Common reaction conditions for hydrogenolysis are a temperature between 440 and 700 K, a pressure between 20 and 180 bar, a high stirring rate, a small catalyst size, and a catalyst weight ratio of around ten.

The main problems currently are its sensitivity to materials which can deactivate the catalyst [13] and the high price of the catalyst. The sensitivity of the catalyst to deactivation can be solved by carefully separating the feedstock from unwanted materials, adding materials that can neutralise unwanted materials or first thermocracking the plastic to create a pure feed of hydrocarbons [13].
One specific example is that polyvinyl chloride (PVC) contains chloride which deactivates the catalyst. This could be solved by, for instance, adding $CaO/Ca(OH)_2$ which neutralises hydrogen chloride into $CaCl_2$ [13]. Because of these reasons, hydrogenolysis can best be paired with good (mechanical) separation techniques to get a pure plastic feedstock and first thermocracking it to remove some of the additional unwanted materials. The process generates a hydrocarbon feedstock that is relatively pure. This can be efficiently transformed into the desired products due to the high selectivity of the catalyst.

After the hydrogenolysis process, the most desirable outcome is a naphtha stream. This is not only because of its economic value, but also because it serves as a suitable feedstock for a steam cracker. The steam cracker produces monomers that can then be utilised to create new polymers. This closes the carbon cycle which is needed for long-term sustainability.

3.2 Hydrogenolysis mechanism

The chemical process consists of the hydrogenolysis of polyolefins to olefins and small alkanes at elevated temperatures in the presence of hydrogen and a catalyst [7, 9, 13]. In this thesis, hydrogenolysis is used to describe the overall chemical reaction while cracking is used to describe the splitting of one compound into two.

Hydrogenolysis is done in the presence of a catalyst because it will reduce the activation energy required for the reaction which would otherwise not happen at the usual temperature. Plastics are usually polyolefins made up of long carbon chains surrounded by hydrogen atoms [12]. When a polyolefin cracks, it is the carbon-carbon bond which breaks (cracking) [10] and both carbons bond with a hydrogen atom (formation).

For solid catalysts, the chemistry of hydrogenolysis is that hydrocarbons will adsorb onto the catalyst surface and are able to react in certain ways with the hydrogen atoms it. This can be seen in figure 3.1.

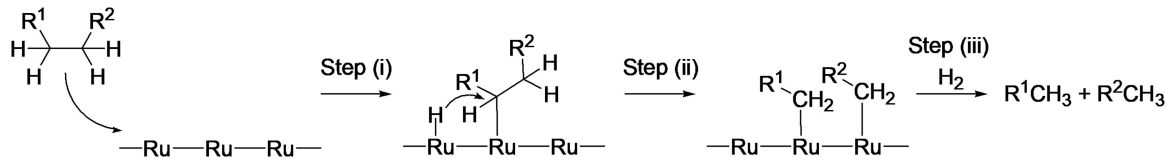

Figure 3.1: General reaction mechanism of hydrogenolysis for hydrocarbons on the ruthenium catalyst surface [12]

First, the hydrocarbon and hydrogen must adsorb onto the catalyst surface in proximity to each other. The larger hydrocarbons will have more trouble getting into the smaller pores of the catalyst so they often react on the catalyst surface [9, 14]. According to Nakaji et al. (2021) [12], who built on their previous work [18, 19], during the adsorption process, the C-H bonds of alkanes are dissociated. This implies that the C-H bond is replaced by two bonds with the catalyst.

In the second step, the C-C bonds dissociate to form two alkyl products on the catalyst surface. This happens with the help of two hydrogen atoms near the hydrocarbon that attack the carbon atom which forces the C-C bond to break.

Finally, the species desorb from the catalyst surface with the help of two hydrogen atoms. They can now leave the catalyst or go deeper into the pores of the catalyst, if the catalyst has pores, where they react further [8]. For the type of catalyst, often acidic zeolites are chosen because of their large pore size and hydrogenolytic abilities [20]. High acidity can also cause a larger selectivity towards gas products [8], which is often undesirable. According to Nakaji et al. (2021) [12], the second step is the rate-determining step if the concentration of the alkyl species on the catalyst is low owing to the weak interaction of C-H of alkanes and the catalyst.

Some literature research assumes that there is an abundance of hydrogen on the catalyst compared to the alkanes. In this research, this is not assumed to be the case and the influence of the hydrogen concentration has been added to the model.

The hydrocarbons crack into different kinds of alkanes. It can crack into two linear carbon chains, loose carbons (methane), and branched products. This is discussed in more detail in the appendix section A.1. Only linear carbon chains will be assumed in this thesis.

Some molecules react faster than others or are formed more likely than others. According to Chen et al. (2022) [10] the rate of hydrogenolysis is affected by the chain length because the adsorption energy required is affected by van der Waals forces with the catalyst and entropic factors. This implies that larger hydrocarbons will react faster on the catalyst surface than smaller ones because they adsorb faster on the catalyst surface. They do, however, find it more difficult to get into the pores of the catalyst and therefore, will not be able to use the catalyst surface as effectively as smaller hydrocarbons. More on this will be explained in section 3.4.

3.3 Mathematical description of hydrogenolytic mechanism

To model the hydrogenolysis of plastic, a set of differential equations for each compound can be made. In literature often a 'lumped' kinetic model is made where groups of hydrocarbons are grouped together [9]. The equations used in this thesis were based on the work of Marathe [15, 16] et al. (2019a, 2019b) who wrote a mathematical cracking model for the pyrolysis of bio-organic compounds but it can be used for any hydrogenolytic mechanism of hydrocarbons. It is a first-order mechanism that focuses on the hydrogenolysis of the individual compounds and redistributes the products evenly over all smaller compounds. This method keeps the mass constant over time which is important for accurate modelling.

Marathe [15, 16] et al. (2019a, 2019b) state that all bonds crack at the same rate. However, in this thesis, it is assumed that bonds of distinct compounds crack at different rates due to selectivity. The bonds within any molecule do still have the same rate of breaking. For any alkane, a compound with length i breaks into a smaller compound j and another compound of the remaining length difference between i and j. This can be seen in equation 3.1.

$$DP_i \rightarrow DP_j + DP_{i-j} \qquad (i > j) \wedge (i > 1) \wedge (j > 0) \tag{3.1}$$

In this equation, DP_i stands for the degree of polymerisation and represents the length of the compound. The compound DP_i can crack in $\frac{(i-1)!}{(i-2)!} = (i-1)$ different ways.

When each bond in a compound cracks at the same rate, the overall rate R_i^c (mole/s) of a single bond cracking is determined by the kinetic rate constant (s^{-1}) of that specific bond and the quantity (mole) of the compound in the liquid:

$$R_i^c = k_i \cdot n_{i,L} \tag{3.2}$$

The amount of moles ($n_{i,L}$) can be used instead of the concentration because it allows for the calculation of the gas and liquid volumes during the reaction if there is no solvent present, more on this in chapter 4. This assumes that density changes do not affect the conversion.

The rate at which a compound cracks is linear to its size. This can be described as:

$$K_i^c = (i-1) \cdot R_i^c = (i-1) \cdot k_i \cdot n_{i,L} \tag{3.3}$$

The total rate of hydrogenolysis for a compound is denoted by K_i^c (mole/s) in this equation.

Every component has a specific rate of cracking and formation, with each bond in a compound having the same cracking rate. The total rate of a compound's cracking is the sum of its individual bond cracking rates. Meanwhile, the formation of a compound is determined by the sum of the total cracking rates of all larger compounds. When a compound undergoes hydrogenolysis, it results in the formation of two compounds. As a result, the rate of this reaction is doubled and can be seen as:

$$K_i^f = 2 \cdot \sum_{j=i+1}^{i_{\max}} k_j \cdot n_{j,L} \tag{3.4}$$

In this equation, K_i^f (mole/s) is the formation rate of compound I. The total differential equation for every compound can be made by combining equations 3.3 and 3.4 into:

$$K_i = K_i^f - K_i^c \tag{3.5}$$

$$= 2 \cdot \left(\sum_{j=i+1}^{i_{\max}} k_j \cdot n_{j,L} \right) - (i-1) \cdot k_i \cdot n_{i,L} \tag{3.6}$$

$$= 2 \cdot \left(\sum_{j=i+1}^{i_{\max}} \frac{k_{j,tot} \cdot n_{j,L}}{j-1} \right) - k_{i,tot} \cdot n_{i,L} \tag{3.7}$$

Here, $k_{i,tot} = k_i \cdot (i-1)$ is the total kinetic rate constant (s^{-1}) of a compound. It is important to note that the total rate of hydrogenolysis (in mole/s) for a compound is represented by the product of $k_{i,tot}$ and $n_{i,L}$. This value is the sum of the rates of all the bonds present in the compound, for the amount of that compound in the liquid phase.

3.4 Mass transfer limitation

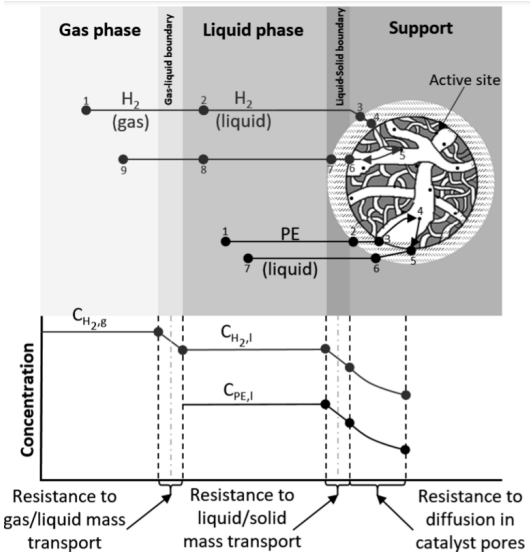

Figure 3.2: Mass transfer resistances for three-phase hydrogenation reaction[9]

A typical hydrogenolysis reaction occurs in a gas/liquid/solid system, where the solid is most often a porous catalyst in the liquid hydrocarbon mixture. Here, there are of course multiple mass transfer limitations [9, 14]. The liquid hydrocarbons travel towards and inside the catalyst to reach the active metal sites. Getting through the pores is difficult for the larger molecules due to their size, which means that these compounds will not be able to use the catalyst as effectively as some of the smaller molecules. There is also a gas phase which at the beginning of the reaction consists of pure hydrogen which dissolves into the liquid phase where it reacts on the catalyst surface Some of the lighter hydrocarbons like methane will evaporate into the gas phase and will not be able to react there in the absence of the catalyst. There might also be some concentration gradients within the gas and liquid phases that could slow down the reaction. All of these transport processes can be seen in figure 3.2.

These mass transport limitations are important because they can help us determine the rate-limiting step in the reaction. This rate-limiting step can either be one of these mass transfer limitations or the reaction rate itself. For the reaction rate, the adsorption and desorption steps are not included based on the work of Nakaji et al. (2021) [12] meaning that these steps are assumed not to be the rate-determining step.

3.4.1 Smaller mass transport limitations

The first mass transfer limitations that will not have a large impact are the gas and liquid concentration gradients. Gas phases have relatively high diffusion rates [21] which are three magnitudes 10^3 larger than liquids and ten magnitudes 10^{10} larger than solids. In the reactor, hydrogen gas makes up the majority of the gas phase for a significant duration. Because of this, it can easily be regarded as a minimal factor and will not be taken into account.

Although liquid diffusion is slower than that of the gas phase, the mixture is well-stirred by the stirrer and there are a large number of catalyst particles present, resulting in a minimal distance between the bulk liquid and the catalyst particles. This implies that also for the liquid phase, the concentration gradient can be neglected. This is also done in the works of Nakaji [12] and Fuentes-Ordóñez et al. (2013) [14].

The final mass transport limitation that will be neglected is the liquid-solid external diffusion. This process could be the rate-limiting step under certain conditions but it is not done in this thesis because of its difficulty to determine accurately and it being neglected in other papers, especially at the reaction conditions used in this thesis, which will be described in chapter 4. Fuentes-Ordóñez et al. (2013) [14] has found that the liquid-solid resistance only affects the reaction at higher viscosity, temperature, molecular weight, pressure, and catalyst size.

This implies that the only mass transport limitations which will be considered in this thesis are the gas-liquid boundary and the internal diffusion within the catalyst. These are described in the sections 3.4.2 and 3.4.3, respectively.

3.4.2 Internal diffusion

Internal diffusion determines how well the compounds can travel within the pores of the catalyst to use the catalyst as effectively as possible [9, 14]. The effectiveness of a compound is influenced by both the rate of diffusion and the speed of the chemical reaction. When the reaction is slow and the diffusion rate is high, the catalyst functions optimally without any major mass transfer impediments [22]. However, if the reaction rate is fast and the diffusion is slow, the internal diffusion may become the rate-limiting factor. The ratio of reaction rate to diffusivity is calculated by the Thiele modulus [23] and can be seen in equation 3.8, assuming first-order reaction for the hydrocarbons and order m for hydrogen.

$$\phi_i = \frac{R_c}{3}\sqrt{\frac{k_{i,tot} m_c \frac{1}{1+m} C_{H_2}^{m-1}}{\rho_c D_{\text{eff},i}}} \tag{3.8}$$

In this equation, R_c is the radius (m) of the catalyst particle, $k_{i,tot}$ is the reaction constant (s^{-1}) as determined in section 3.2, ρ_c is the density (kg/m^3) of the catalyst, m_c is the mass (kg) of the catalyst particles, $C_{H_2}^{m-1}$ is the hydrogen concentration (mol/m^3) to the power m minus 1, and $D_{\text{eff},i}$ is the effective diffusion (m^2/s). The effective diffusion is calculated with equation 3.9:

$$\frac{1}{D_{\text{eff},i}} = \frac{\tau}{\epsilon}\left(\frac{1}{D_{K,i}} + \frac{1}{D_{M,i}}\right) \tag{3.9}$$

Here, τ is the tortuosity which is the shape of the pore or the 'detour' [24] a molecule must take within the catalyst. The porosity of the catalyst molecules is described by ϵ and is the fraction of the catalyst volume that is empty for particles to travel through [24]. Due to these factors, diffusivity is affected. The total diffusion is the smallest of two types of diffusion: Knudsen diffusion and molecular diffusion. Knudsen diffusion is the diffusion when the molecules 'bump' [24] against the pore surfaces more frequently than against other molecules within the pores. If the molecules are very large or the pore size is small then the Knudsen diffusion will be more influential than the normal molecular diffusion $D_{M,i}$. The Knudsen diffusion is calculated with equation 3.10.

$$D_{K,i} = \frac{d_p}{3}\sqrt{\frac{8RT}{\pi M_{w,i}}} \tag{3.10}$$

In this equation, d_p is the pore diameter (m), R is the gas constant (J/mole/K), T is the temperature (K), and $M_{w,i}$ is the molecular weight (g/mole) of the molecule.

The final effectiveness of the catalyst is calculated by equation 3.11 for spherical catalyst particles [24].

$$\eta_i = \frac{3}{\phi_i}\left(\frac{1}{\tanh\phi_i} - \frac{1}{\phi_i}\right) \tag{3.11}$$

The ultimate efficiency is influenced by various parameters, often including pressure. However, pressure is excluded as Knudsen diffusion is not dependent on it. Such is the assumption made in this thesis.

3.4.3 Evaporation

The reaction happens in the liquid active phase, which consists of the polymer, smaller hydrocarbons and catalyst particles. This liquid phase is in equilibrium with the gas phase which, at the beginning of the reaction, consists of pure hydrogen. This hydrogen gas slowly dissolves into the liquid phase as hydrogen is consumed over the course of the reaction. While hydrogen dissolves into the liquid phase, small hydrocarbons such as methane evaporate into the gas phase. The differential equation for the evaporation and dissolving is given by the equation below:

$$\frac{\mathrm{d}n_{i,G}}{\mathrm{d}t} = k_L a_i \cdot (C_i^* - C_{i,G}) \tag{3.12}$$

Here, $k_L a_i$ is the volumetric evaporation rate (m^3/s), C_i^* representing the concentration ($mole/m^3$) of the component at the gas/liquid interface, and $C_{i,G}$ the concentration ($mole/m^3$) in the bulk gas phase. The concentration at the gas/liquid interface is calculated with the modified ideal gas law:

$$C_i^* = \frac{P_i^* x_i}{ZRT} \tag{3.13}$$

With P_i^* being the vapour pressure (Pa), x_i the mole fraction in the liquid phase, Z the compressibility factor, R is the gas constant (J/mole/K), T is the temperature (K).

The vapour pressure, for some compounds, was calculated with the relation between the vapour pressure and the temperature, similar to the Antoine equation:

$$\log_{10} P_i^* = A + \frac{B}{T} + C\log_{10} T + DT + ET^2 \tag{3.14}$$

This formula was used for hydrocarbons between C5 and C13 (five and thirteen carbon atoms long) because the vapour pressure for smaller compounds is only calculated at temperatures lower than the reaction temperature. Based on the reduction in vapour pressure with molecule size, it is assumed that C13 is the largest compound that will evaporate. This assumption is made to simplify the model and is

also done by Bin Jumah et al. (2021) [9] who identified naphtha as the highest evaporating compound, with a maximum of C13. Henry's law was used for hydrogen and the smallest four hydrocarbons because it could describe these vapour pressures at higher temperatures. It is also more useful for calculating the vapour pressure when there are many compounds in the mixture. The vapour pressures from Henry's law in the mixture are calculated with Aspen Plus V12 using equation 3.15.

$$He_i = \frac{P \cdot y_i}{x_i} \tag{3.15}$$

In this equation, He_i is the Henry constant (Pa) for component i, P is the total pressure (Pa) and y_i and x_i are the molar fractions in the gas and liquid phases respectively.

The last part is the evaporation rate $k_L a_i$ (m^3/s). Because the hollow-shaft stirrer used in the practical experiments sucks the gas into the liquid, gas bubbles are formed in the liquid. This implies that the surface area of the gas-liquid interface is very high and impossible to calculate. Due to this, the $k_L a_i$ value will be calculated by the model.

It is possible to calculate the ratio of evaporating compounds. The largest resistance towards the equilibrium interface is the diffusion between this interface and the liquid side because liquid diffusion is slower in comparison to gas diffusion [21]. The ratio in the evaporation rate $k_L a_i$ will therefore be the ratio between the liquid diffusion of the compounds [9]. If the model is capable of predicting one, it will predict all of them at the same time. This is expressed in equation 3.16.

$$k_L a_i = \frac{D_i}{D_j} k_L a_j \tag{3.16}$$

With $k_L a_i$ as the volumetric evaporation rate (m^3/s), D_i the liquid diffusion (m^2/s), and $k_L a_j$ as the volumetric evaporation rate of a different compound which can evaporate. The liquid diffusion is calculated by the Scheibel equation [25] because it does not use a specific solute-solvent interaction parameter like the Wilke-Chang equation which makes it easier to calculate the diffusion ratio. The Scheibel equation can be seen in equation 3.17.

$$D_i = \frac{8.2 \cdot 10^{-8} T}{\eta_{\text{solv}} V_{i,\text{mol}}^{1/3}} \cdot \left(1 + \left(\frac{3V_{\text{solv,mol}}}{V_{i,\text{mol}}}\right)^{2/3}\right) \tag{3.17}$$

In this equation, η_{solv} is the viscosity $(Pa \cdot s)$ of the solvent, which is the mixture, and $V_{i,mol}$ is the molar volume $(m^3/mole)$ of the liquid solute at its normal boiling point [25]. Since only the ratio of the different diffusion rates was needed, the formula can be simplified further as can be seen in equation 3.18.

$$\frac{D_i}{D_j} = \frac{V_{j,mol}^{1/3} + V_{j,mol}}{V_{i,mol}^{1/3} + V_{i,mol}} \tag{3.18}$$

Now the diffusion ratio only depends on the molar volume.

Total hydrogenolysis rate

The hydrogen dissolves from the gas phase into the liquid phase as is determined in section 3.4.3. The reaction order for the hydrocarbons was set to be one as is done in similar works [9, 14, 15, 16]. The reaction order for hydrogen would have to be predicted by the model. The hydrogenolysis rate can now be written as equation 3.19.

$$K_i^c = k_{i,tot} \cdot n_{i,L} \cdot n_{H_2,L}^m \cdot \eta_i \tag{3.19}$$

In this equation, m is the reaction order for hydrogen.

The total rate of a hydrocarbon in the liquid phase, which includes formation, cracking, and evaporation, can be seen in equation 3.20. More detailed information on all the differential equations can be found in section A.2 of the appendix.

$$\frac{\mathrm{d}n_{i,L}}{\mathrm{d}t} = 2 \cdot \left(\sum_{j=i+1}^{i_{max}} \frac{k_{j,tot} \cdot n_{j,L} \cdot n_{H_2,L}^m \cdot \eta_j}{j-1}\right) - k_{i,tot} \cdot n_{i,L} \cdot n_{H_2,L}^m \cdot \eta_i - \frac{\mathrm{d}n_{i,G}}{\mathrm{d}t} \tag{3.20}$$

3.5 Density

To calculate the evaporation rate, the concentration in the gas bulk was calculated with the volume of the gas. However, because density and evaporation changes over time, the volumes of the gas and liquid phases change over time. This is because the polymer cracks into smaller compounds which have a lower density. The volumes are calculated by the fixed reactor volume and the density of the liquid components and their respective mass fractions in the liquid phase as can be seen in equation 3.21.

$$\rho = \sum_{n=1}^{n_{max}} x_i \cdot \rho_i \tag{3.21}$$

The volume (m^3) of the liquid and gas can now be calculated from the density ρ (kg/m^3) and the mass (kg) of each component.

$$V_L = \frac{\sum_{n=1}^{n_{max}} m_i}{\rho} \tag{3.22}$$

$$V_G = V_{total} - V_L \tag{3.23}$$

3.6 Compressibility

In order to make the evaporation process more detailed, the compressibility of the gas was determined. The compressibility was calculated using the Peng-Robinson equation of state which is a modified van der Waals equation. This is a two-parameter cubic equation of state in volume which depends only on the critical temperature and critical pressure of the gas. This equation is also used in the Aspen+ model and in similar modelling [26]. The formula is given as:

$$P_{real} = \frac{RT}{V_m - b} - \frac{a\alpha}{V_m^2 + 2bV_m - b^2} \tag{3.24}$$

With V_m as the molar volume ($m^3/mole$) in the gas phase, a ($m^3 \cdot J/mole^2$) and b ($m^3/mole$) as the calculated attraction and repulsion parameters, and α as the acentricity component (-) [27]. The parameters and factors for equation 3.24 are calculated as:

$$\alpha = \left(1 + k \cdot \left(1 - T_r^{0.5}\right)\right)^2 \tag{3.25}$$

With T_r as the reduced temperature (-) relative to the critical temperature (K).

$$k = 0.37464 + 1.54226 \cdot w - 0.26992 \cdot w^2 \tag{3.26}$$

The term k is used for simplification (-), while w represents the non-sphericity (centricity) of the molecule as the acentric factor (-).

$$a = 0.45724 \cdot \frac{R^2 T_c^2}{P_c} \tag{3.27}$$

$$b = 0.07780 \cdot \frac{RT_c}{P_c} \tag{3.28}$$

The total compressibility factor Z (-) is calculated by:

$$Z = \frac{P_{real}}{P_{ideal}} \tag{3.29}$$

For mixtures of two different compounds the $a\alpha$ and b values change and are calculated with the equations below [28].

$$b_m = \sum_{i=1}^{2} z_i b_i \tag{3.30}$$

$$a_m \alpha_m = \sum_{i=1}^{2} \sum_{j=1}^{2} z_i z_j (1 - k_{i,j}) \sqrt{a_i \alpha_i \cdot a_i \alpha_i} = (1 - k_{i,j})(z_i \sqrt{a_i \alpha_i} + z_j \sqrt{a_j \alpha_j})^2 \tag{3.31}$$

In this equation, $k_{i,j}$ is the binary interaction parameter (-) [28] and z_i is the molar fraction of that component (-).

Chapter 4

Method

Here, the process modelled in this thesis is described in terms of the experimental set-up, materials used, reaction conditions, assumptions, research method, model description, and differential equations. Based on the information here the model can be replicated. The experimental data was supplied by IR. E. van Daatselaar who is a PhD student in the Sustainable Process Technology group of the University of Twente and who is the daily supervisor in this bachelor thesis.

4.1 Experimental

The used polymer is 3.5 grams of LDPE (MW $\sim$ 4 kDa; Mn $\sim$ 1.8 kDa) supplied by Sigma-Aldrich Corporation [29] and is used as received. It is mixed with 0.39 grams of 5 wt% Ru/C catalyst (product number 206180) supplied by Sigma-Aldrich Corporation [29] which is chosen because of good reactivity and internal surface area.
It is placed in a 45 ml stirred batch reactor (autoclave) of which 41.5 ml is the available empty volume for the reaction due to the size of the hollow-shaft mechanical stirrer.
The reactor is under 40.1 bar pure hydrogen (0.118 mole hydrogen) pressure which increases to 65 bar under the reaction temperature of 523 K. Unless otherwise suggested, these reaction conditions will be assumed throughout the entirety of the thesis and will therefore not be repeated. More information about the experimental process and the experimental measurements can be seen in section B.1 of the appendix.

The respective yields were calculated from the obtained mass fractions compared to the feed polyolefin and the calculations can be seen in figure B.1 of the appendix section B.3. The difference between the mass of the product and the quantified mass is said to consist of C34 and greater. This makes modelling difficult because the starting material for this model is assumed to exclusively exist of C200, meaning that C34 to C200 are grouped together to compare the model results to the experimental values. This also means that the conversion could not be determined accurately.

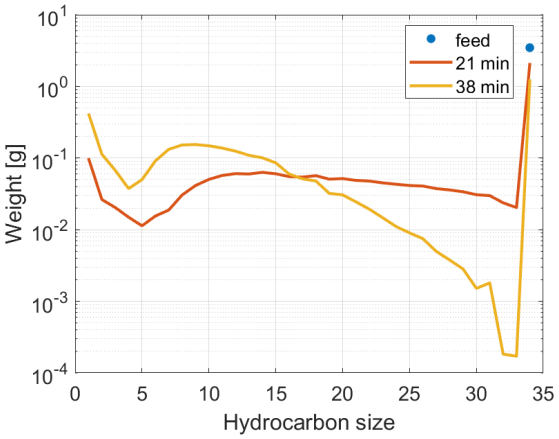

Figure 4.1: Experimental results distribution and feed over time. C34+ is grouped together

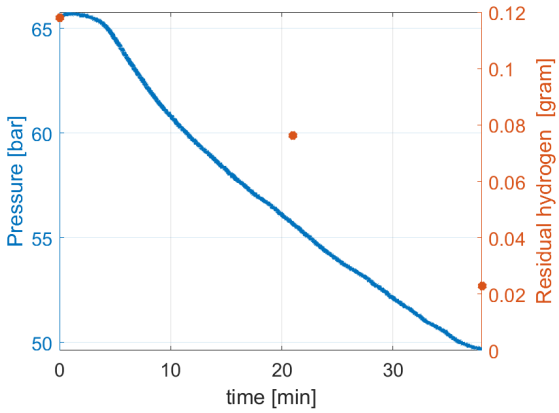

Figure 4.2: Pressure (blue, left axis) and residual hydrogen (orange, right axis) experimental data over time

The experimental data obtained consists of the weight distribution of the reaction and residual hydrogen at two points in time (21 and 38 minutes), and the measured pressure during the entire reaction. This can be seen in the figures 4.1 and 4.2. Hydrocarbon size refers to the number of carbon atoms. It's worth highlighting that pressure and residual hydrogen are represented on the same graph, but we can't draw a direct correlation between them because they exist on different axes and have different magnitudes

of decrease. This makes it tricky to interpret any potential linear relationship so it's important to take caution when making any direct conclusions.

The goal of the model is to predict these experimental results as closely as possible. The evolution of the weight distribution over time can be seen in figure B.2 of the appendix B.3.

4.2 Parameters

Catalyst and compressibility values
The exact characteristics of the catalyst were not supplied by the manufacturer. For the model, literature values were chosen instead. This does mean that the calculated effectiveness is not representative of this specific reaction but is a suggested value based on average Ru/C catalyst characteristics. The chosen values can be seen in table 4.1.

Table 4.1: Ru/C catalyst chosen characteristics

Parameter	Abbreviation	Unit	Source
Average pore diameter	d_p	30 nm	[30]
Tortuosity	τ	3	[31]
Porosity	ϵ	0.3	[31]
Particle radius	R_c	139 μm	[9]
Density activated carbon	ρ_c	34.4 kg/m^3	[32]

The units that are used in the calculations for the compressibility can be seen in table 4.2. It is assumed for the compressibility that the gas phase consists of only hydrogen and methane, with methane being the sum of all hydrocarbons in the gas phase.

Table 4.2: Compressibility parameters between hydrogen and methane for the gas phase

Parameter	Abbreviation	Unit	Source
Critical temperature hydrogen	T_c	33.14 K	[33]
Critical temperature methane	T_c	190.564 K	[33]
Critical pressure hydrogen	T_c	12.964 bar	[33, 34]
Critical pressure methane	T_c	45.992 bar	[33]
Acentric factor hydrogen	ω	-0.216	[35]
Acentric factor methane	ω	0.011	[35]
Binary interaction parameters	$k_{i,j}$	0.05	[28]

Evaporation
The calculations for the diffusion ratio for the evaporation process are based on the molar volume which requires the density and the molecular weight. This density can be seen in table 4.3. A pressure value of 60 bars instead of 65 bars was used to give a more accurate representation of the average pressure over the course of the reaction.

Table 4.3: Density (kg/m^3) of evaporating compounds at boiling point and 60 bar [33]

C1	C2	C3	C4	C5	C6	C7	C8	C9	C10	C11	C12	C13	H2
427.6	549.4	587.33	608.54	617.7	622.2	624.0	623.2	620.4	616.6	598.6	609.0	604.8	76.86

The vapour pressures for each compound can be seen in figure 4.3. As can be seen here, the vapour pressure decreases exponentially with hydrocarbon length. The values from Henry's law and the Antoine equation form an almost straight line in the logarithmic plot. The vapour pressure for pentane is a little bit above this line which is most likely caused by the use of a different equation at this point.
The vapour pressure for hydrogen was determined by Henry's law and calculated with an Aspen Plus model of a flash vessel. It was found to be 449.3 bar. This is logical because it should evaporate much faster than even the smallest hydrocarbon methane, which has a Henry coefficient of 287 bar.
At a temperature of 523 K and pressure of 60 bar, hydrocarbons smaller than hexane reach their boiling point and exist naturally in the gas phase if no restrictions from mass transport or pressure increase apply.

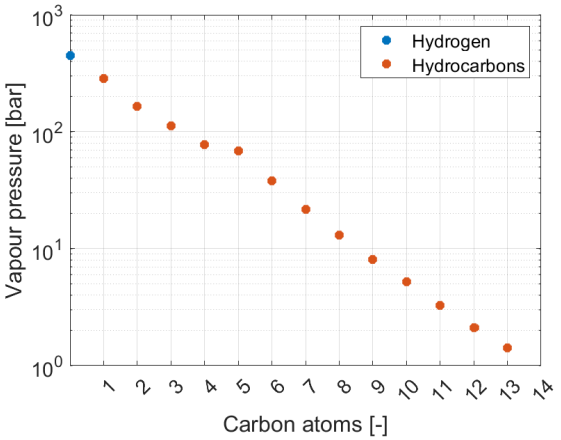

Figure 4.3: Vapour pressures hydrocarbons and hydrogen at 60 bar and 523K

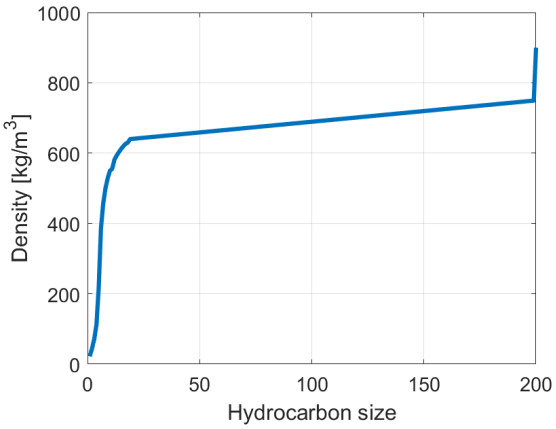

Figure 4.4: Density per liquid hydrocarbon at 60 bars and 523K [33]

Density

The density of each component until $C_{18}H_{38}$ was calculated at 60 bar pressure and 523 K using the NIST website [33] and are used for the entire reaction process, also when the pressure decreases for simplification. These are the initial conditions and this is again done for simplification. The other densities were interpolated between 640 and 750 kg/m^3 and the final one represents the polymer with a density of 910 kg/m^3 [36]. The densities can be seen in figure 4.4.

It can clearly be seen that the difference between the average density and the density of the smallest components is quite large. This is logical because these compounds have very little mass in comparison to the distance between molecules which is roughly the same for all compounds and is based on the temperature. For the larger compounds, this difference is relatively small because the mass and distance between molecules are small in relative terms.

The smaller compounds will most likely evaporate largely into the liquid phase so should not have a large impact on the overall density. Hydrogen has a density of 2.72 kg/m^3 [33]. With the density known, the volume of the liquid was calculated based on the masses of the liquid components. The volumes are calculated from the reactor volume which is 41.5 ml using equation 3.23.

4.3 Model and calculations

The reaction was modelled in Matlab R2022b and uses the ODE15s solver with relative and absolute tolerance, which is allowed for the computational accuracy of the variable-step solver [37], of 10^{-6}. The fitting program used is lsqcurvefit which is a nonlinear curve-fitting (data-fitting) program [38] which calculates the least squares between the experimental data and the fitted values from the model. The function tolerance for the regression was set to 10^{-8}.

The model itself consists of four different parts: pre-calculations, the regression programme, a function with differential equations, and post-calculations. More on this can be seen in section B.2 of the appendix.

Differential equations

The model describes the reaction by recognising that the system consists of two physical phases, i.e. gas and liquid. It was assumed that there is no concentration gradient within the gas and liquid phases and that the mass transport limitation between the liquid and the catalyst interface was not rate determining as explained in chapter 3. Knudsen diffusion is assumed to be dominant as a simplification.

The complete differential equation for hydrocarbons in the liquid phase can be seen in equation 4.1.

$$\frac{\mathrm{d}n_{i,L}}{\mathrm{d}t} = 2 \cdot \left(\sum_{j=i+1}^{i_{max}} \frac{k_{j,tot} \cdot n_{j,L} \cdot n_{H_2,L}^{m} \cdot \eta_j}{j-1} \right) - k_{i,tot} \cdot n_{i,L} \cdot n_{H_2,L}^{m} \cdot \eta_i - \frac{\mathrm{d}n_{i,G}}{\mathrm{d}t} \tag{4.1}$$

For the model, it is assumed that every C-C bond within a polymer has the same rate of breaking. This implies that selectivity towards specific regions of the hydrocarbon is not taken into account. The balance was set up as a mole balance instead of a concentration balance to calculate the volumes during the calculations for better results. It has no impact on the calculated reaction constants.

The reaction constants for C1 to C33 are calculated separately because these compounds have individual yields whereas the groups C34 to C99 and C100 to C199 have one kinetic rate constant per group to limit the number of fitting parameters used. C200 has its own reaction constant.

It was assumed to have first-order reactions for the hydrocarbons. This is also done in literature [9, 14] and means that micro-mixing does not need to be taken into account.

It is also assumed that hydrogen influences the reaction and has a reaction order between zero and one. This is based on the assumption that hydrogen and the hydrocarbons do not compete for the same spot which could cause a negative reaction order for hydrogen and the assumption that the rate does not increase exponentially with increasing hydrogen. Due to a lack of time, the kinetic rate constant was calculated with units $1/s$ instead of $1/s/mole^m$ for simplification. In possible follow-up research, this will need to be taken into account. Density changes will also impact equation 4.1 but this has also been neglected in this thesis for simplification.

The differential equation for the evaporation process can be seen in equation 4.2. The change to the gas phase is subtracted from the liquid phase. This equation counts also for hydrogen.

$$\frac{\mathrm{d}n_{i,G}}{\mathrm{d}t} = k_L a_i \cdot (C_i^* - C_i) \tag{4.2}$$

The differential equation for the amount of hydrogen in the liquid phase can be seen in equation 4.3. The first part is the amount of hydrogen that is used in the hydrogenolysis process. One mole of hydrogen reacts with one mole of cracked material. The second part is the evaporation of hydrogen which is negative because it is from the perspective of the liquid phase.

$$\frac{\mathrm{d}n_{H_2,L}}{\mathrm{d}t} = -\sum_{n=2}^{n_{max}} \frac{\mathrm{d}n_{i,L}}{\mathrm{d}t} - \frac{\mathrm{d}n_{H_2,G}}{\mathrm{d}t} \tag{4.3}$$

Chapter 5

Results and discussion

This chapter discusses all the important reaction conditions and calculated values from the model. It is divided into chapters for each subject similar to the sub-chapters in the theory chapter. The goal is to compare the experimental results to the modelled values and to discuss the accuracy of the results.

5.1 Products results

Mass over time
In figure 5.1, the curved lines represent the fitted values from the model while the dots represent the experimental data. The top purple line represents the C34+ group, which includes the unconverted polymer. It appears that the model can accurately predict the hydrogenolysis rate of this group. It is not surprising that the model finds it easy to predict this group, as it is the largest and therefore cannot be formed by other groups which are all smaller.

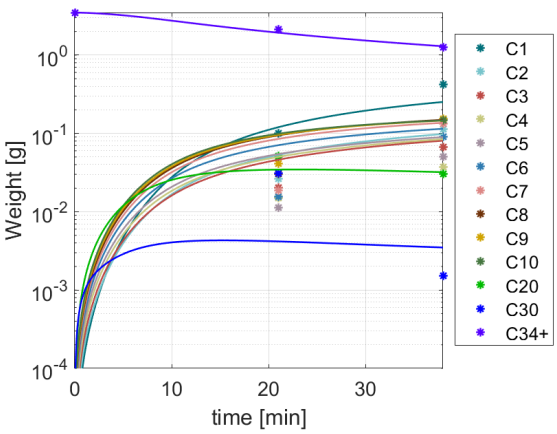

Figure 5.1: Modelled mass (lines) over time against experimental data (dots) for some compounds. C34+ is grouped together.

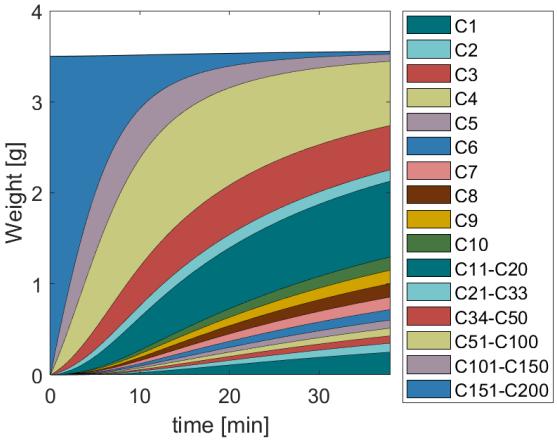

Figure 5.2: Modelled evolution of mass over time. Some compounds are grouped together.

The assumption that compounds can only become smaller is supported by experimental results, which show that there are no larger compounds in the product compared to the feed. The next biggest product in terms of weight is methane which the model predicts very well. This is also not surprising since the model can tweak the reaction rates of the smallest components in such a way that the yield of methane can be closely controlled. For the groups C3 to C10, the model can predict the final yield relatively well but appears to overpredict the yields at 21 minutes. This can be expected because regression fitting has a tendency to favour the first and last values when creating the best fit.

Another reason could be that the hydrogen dependence slows the reaction down too much after a certain amount of time which would make the reaction rate at the beginning too high.

C30 favours the final point, with a high yield expected at 21 minutes that should decrease over time. However, the yield remains steady and doesn't reflect this behaviour. This could mean that the reaction rate for C30 is higher but that less of it is formed in the earlier stations of the reactions. In order to better predict the intermediate results during the reaction, more data points would be required.

Another possibility for the lower yield of major products at 21 minutes is that the model tries to increase the consumed hydrogen and lower the pressure, to get a better fit, by reacting away the major products faster at the beginning of the reaction. More on this will be explained in later sections.

Figure 5.2 shows the evolution of certain hydrocarbon groups over time. The model predicts the 33 measured compounds for 2.35 grams, and the experiment showed 2.23 grams, which is similar. The total mass appears to remain constant because of the conservation of mass rules but it actually increases from 3.5 to 3.62 grams because of the added mass from hydrogen to the liquid products. The quantity of moles present increases significantly as can be seen in appendix figure C.5 of section C.5. The yields of the compounds above C100 are negligible compared to the rest which can be supported by the experimental results which show that the viscosity of the liquid is lower than for any polymer. A more detailed version of figure 5.2 can be seen in figure C.6 of the appendix section C.5.

Product result distribution

The result distribution in grams against the experimental data can be seen in figure 5.3. The overall fit looks good which is to be expected since the first 33 compounds have their own reaction constant which makes it easier to fit these exact values. A more detailed comparison of figure 5.3 can be seen in figure C.7 in the appendix section C.5.

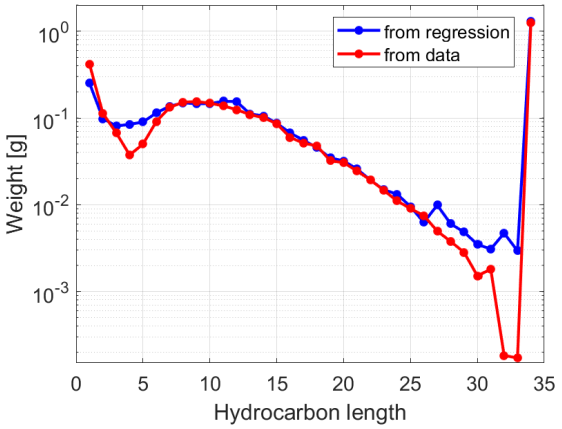

Figure 5.3: Modelled distribution result mass against experimental data. C34+ is grouped together

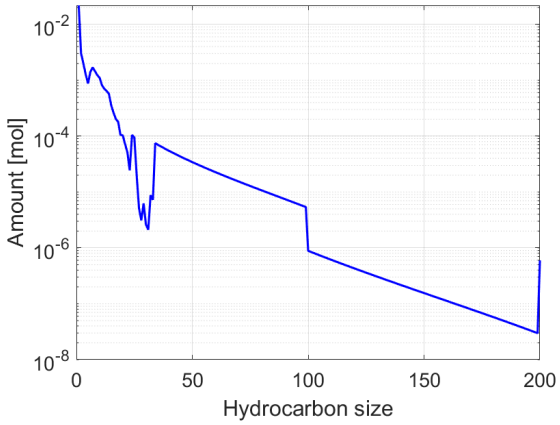

Figure 5.4: Modelled distribution result molar for all hydrocarbons

The molar product distribution can be seen in figure 5.4. The yield clearly decreases with size which can be explained by the hydrogenolytic system, as explained in section 3.2, which cracks a compound and then distributes it equally among all smaller components. Since the smallest compounds have more different ways of getting formed it is logical that these have a higher yield. The curved lines from C34 to C99 and from C100 to C199 can be explained by the fact that these groups of compounds have the same kinetic rate constant.

The yield of C4 to C6 is predicted higher by the model. It is likely that the amount measured in this range is underestimated by the measuring equipment because the two different measurement methods overlap in this area, making it harder to accurately predict the yield. This is because both measurement techniques could struggle to predict the yields of the largest and smallest compounds in their range, resulting in a lower yield in the overlapping area. The overlap can be seen in figure C.8 of appendix section C.5. The gas phase is measured with GC while the liquid phase is measured with GC-MS.

The yield of C27 to C33 is also predicted higher by the model, likely because it is also underestimated by the experimental measurements as discussed above. This is also supported by the fact that if the decrease in yield continued beyond C33 is extrapolated at the same rate, the yield of the C34+ group would have to be a lot smaller. This can also be seen in figure C.7 of the appendix section C.5.

If the yield of C4 to C6 and C27 to C33 are indeed higher than measured, the yield of the C34+ group should be lower. The reason for this is that the latter group's calculation relies on the total quantified yield. If the yield is incorrect, it will result in a lower total yield for C34+. The equation for the yield can be seen in figure B.1 in the appendix section B.3.

The composition of the liquid and gas phases is discussed in appendix section C.1. The conversion of the polymer is found to be likely above 97%. This is discussed in more detail in the appendix section C.2.

5.2 Pressure and density

Density

The density of the liquid can be seen in figure 5.5. The density starts at 900 kg/m^3 because it consists only of the polymer and hydrogen at the beginning and the density is calculated in weight fractions, see section 3.5. It decreases quickly as the largest compounds are broken up and the average molecular weight decreases because smaller compounds have less weight in comparison to the distance between molecules. This can be seen in figure C.12 of the appendix section C.5. The density decrease slows down over the course of the reaction because the difference in the compound size becomes smaller over time. This is to be expected since the reaction process is assumed to only make compounds smaller over time. At the end of the reaction, the density has decreased to 590 kg/m^3 which is roughly the same as for C13 which has 593.1 kg/m^3 at 523 K and 60 bar [33] meaning C13 is the average molecular weight, slightly higher compared to naphtha.

Throughout the reaction, the density at 60 bars was presumed, even if the pressure dropped to 50 bars, as any density changes were negligible. At 50 bars and 523 K, C13 has a density of 590.3 kg/m^3 which is only 2.8 kg/m^3 less. It can therefore be assumed that the density is accurate.

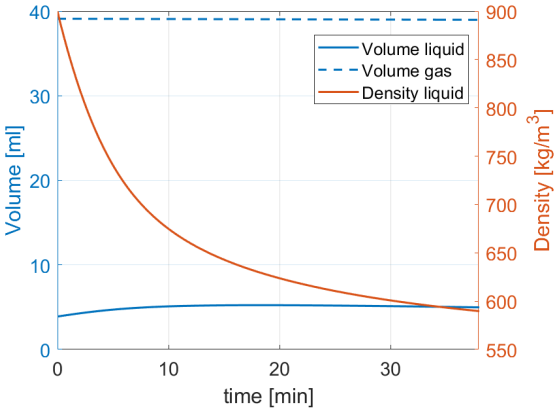

Figure 5.5: Modelled volume of both phases and liquid density over time

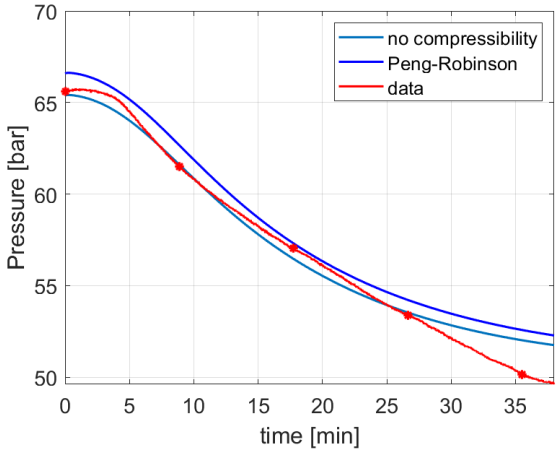

Figure 5.6: Modelled pressure with and without compressibility against experimental results

Volume

The volume of both phases can also be seen in figure 5.5. The volumes depend on the fixed total volume of the reactor and the composition of the liquid phase and the density of the mixture as calculated in section 3.5. It can be seen that the volumes of the two compounds stay roughly the same. This can be explained by the fact that while the density of the liquid decreases, some of its components evaporate into the gas phase which balances it out. Therefore the assumption that a mole balance could be made is mostly accurate, because of a constant liquid volume. The constant volume is also found in other works in this field [9].

Pressure and compressibility

The pressure over time from the experimental results and the regression can be seen in figure 5.6. The red dots represent the data points where the model is fitted against the experimental results. This was chosen because the pressure would otherwise be too dominant in the regression process because of its many data points. It should be noted that an initial amount of 0.118 grams of hydrogen was used instead of the measured 0.124 grams because the pressure at the initial points would otherwise not have lined up, which would mean that the pressure could not be accurately predicted by the model. This could also be caused by a slightly higher reactor volume.

The compressibility of the gas stays roughly the same with $Z = 1.0185$ at the beginning and $Z = 1.0102$ at the end. This is to be expected since the compressibility of hydrogen and methane are both around 1 with methane slightly lower with $Z = 0.9993$ at the end. This matches with the literature [33, 39] and implies that the regular ideal gas law would describe the gas reasonably well. The pressure drops over time because the evaporation rate for hydrogen is higher than the evaporation rates of the hydrocarbons combined as can be seen in figure C.13 of the appendix section C.5.

Pressure fit against experimental data
The fit between the model and experimental results is mostly good. It can clearly be seen that both pressures stay constant initially before decreasing. This is because the hydrogen amount in the liquid phase is first consumed before the concentration gradient between the liquid and gas phases for hydrogen becomes large enough for hydrogen to dissolve into the liquid phase. The decrease in the number of moles in the gas phase results in a reduction of the pressure. According to the model, after 30 minutes, the rate of pressure decrease is expected to slow down due to the additional pressure caused by methane evaporation. However, the actual experimental results indicate only a minimal decrease.

The slight difference in pressure can be explained by a few reasons.
The pressure drops less quickly in the model because C200 was chosen instead of C286 which would require more hydrogen to crack down into the products. With some 'back-of-the-envelope' calculations, using the ideal gas law and average compressibility, this only makes a difference of 0.00038 mol hydrogen which would cause a 0.43 bar pressure difference, which is not enough to explain the gap.
Because the plastic has an average molecular weight of 4000 g/mol, some of its components are larger than C286 but this is unlikely to explain the pressure difference. Molecular weight distribution was not assumed in this thesis.
It could also suggest that the model overestimates the amount of methane which evaporates. The yield of methane is already lower compared to the experimental data in a likely attempt by the regression programme to lower its influence on the pressure. This could suggest that it is not the amount of methane produced but the amount of methane which evaporates that is overestimated by the model. The pressure composition can be seen in figure C.14 of the appendix section C.5.

5.3 Hydrogen

The Aspen+ model determined that at equilibrium conditions, with 3.5 grams of liquid and 0.118 grams of hydrogen, the molar fraction of hydrogen in the liquid was around 14%. This is the case at the start of the reaction. The residual hydrogen in the reactor can be seen in figure 5.7.

Pressure fit against data
The red dots are the experimental results for the beginning of the reaction and two points in time. The dark and light blue lines are for the amount of hydrogen in both phases. The amount of hydrogen in the liquid phase can be seen in more detail in figure 5.8. The amount of hydrogen in the gas phase compared to the liquid phase is 300 times as much at the beginning and 4000 times as much at the end of the reaction. This is explained by the high vapour pressure of hydrogen of 449.3 bar and the mass transport limitations between the gas and liquid phases which is more present at the end of the reaction.

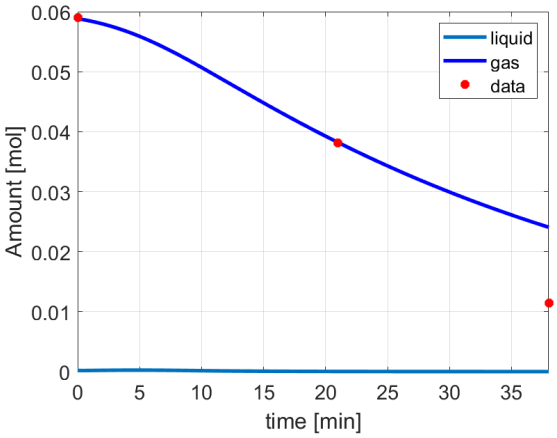

Figure 5.7: Modelled hydrogen amount in both phases against experimental results over time

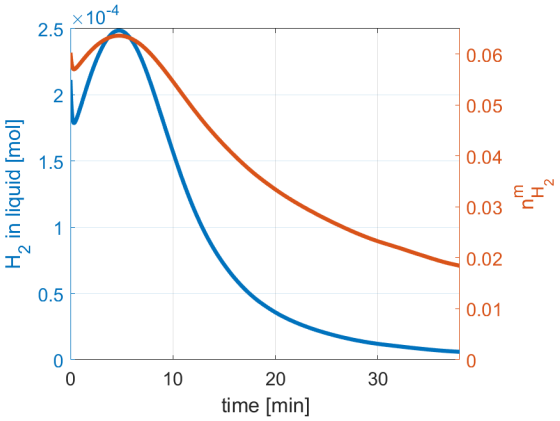

Figure 5.8: Modelled hydrogen in the liquid phase and hydrogen reaction speed influence over time

The total amount of hydrogen consumed by the reaction is 0.0699 grams which is 59.2% of the initial 0.118 grams. This weight is lost because it is added to the total weight of the hydrocarbon mixture which increases from 3.5 to 3.5699 grams. The model can accurately predict the amount of hydrogen left at 21 minutes but fails to predict the amount at 38 minutes. The experimental data says that 81.5% of hydrogen should have been removed from the gas phase, which is a lot more. This can be explained by a few reasons.

The first reason is the dissolvement of hydrogen could be underestimated by the model because the amount of hydrogen in the liquid decreases greatly by the end of the reaction as can be seen in figure 5.8. This is likely because that would also decrease the pressure as discussed earlier, solving two problems at once. Unfortunately because of the fast difference between the amount of hydrogen in the gas and liquid phases, this will not make a large difference.

The second reason is that the yield is biased towards heavier compounds that require less hydrogen. This is due to the fact that the model slightly underestimates the amount of methane, which has the highest hydrogen consumption by weight, as can be seen in figure 5.3. It is also true that no data exists for compounds larger than C33 which could mean that the model can overestimate the amount of larger components in favour of smaller ones. It is unlikely that a significant change will occur in the amount of hydrogen consumed, as the difference in methane yield is only a small portion of the total yield. Moreover, the regression analysis would have already considered the distribution of larger components for a more accurate fit. As can be seen in figure 5.4, the model already predicts that the yield of the larger compounds is relatively small.

The third reason is that the experimental result for the amount of unconsumed hydrogen is wrong and that it should be higher. This is supported by the fact that the model can predict one data point with a high degree of accuracy but the second one very badly. Even though this could be a viable explanation, an error in measurement will not be assumed to be the cause but more data could provide more insight into whether the point is an outlier or not.

The fourth reason for the difference could be explained by the fact that the equipment used can not precisely measure the yield of the materials as discussed in subsection 5.1. This would cause an increase in the yield of smaller compounds which means more hydrogen would be consumed. This is the most logical explanation for the difference because it explains the large gap in the residual hydrogen between the experimental results and the model.

Hydrogen in liquid phase and evaporation

The amount of hydrogen in the liquid phase can be seen in figure 5.8. In the first few seconds, hydrogen is consumed at a high rate before the molar fraction of hydrogen in the liquid phase reaches a low enough point that it drives the dissolvement of hydrogen into the liquid phase. The evaporation rate and hydrogen molar fractions can be seen in figures C.13 and C.15 of the appendix section C.5. After about five minutes, the reaction rate has increased sufficiently, together with the lower hydrogen amount in the gas phase which causes the amount of hydrogen to decrease rapidly. At the end of the reaction, there is 2.81% of the original amount of hydrogen in the liquid phase. It is expected that the hydrogen amount would decrease over time which slows down the reaction speed. But the sharp decrease in concentration is most likely caused by something else.

Hydrogen evaporates in a certain ratio compared to the hydrocarbons which is calculated by the difference in liquid diffusion caused by a difference in molar volume at their boiling points as calculated in section 3.4.3. The assumption that the evaporation ratio between the two is based on the difference in liquid diffusion as calculated by the Scheibel equation could therefore be inaccurate. Bin Jumah et al. (2021) [9] also made the assumption, using the Wilke-Chang equation. However, they only applied this to hydrocarbons that predominantly evaporate rather than dissolve. The assumption could be incorrect because methane evaporates while hydrogen dissolves, this would perhaps require a different formula.

An incorrect evaporation rate would explain the difference in pressure and the sharp drop in hydrogen liquid concentration. Not enough hydrogen can dissolve because if the volumetric evaporation rate is increased too much, methane would evaporate too much, driving up the pressure. Because the methane and hydrogen evaporation rates are linked based on their liquid diffusion ratio, only a fixed amount of hydrogen can dissolve without the amount of methane in the gas phase causing an increase in pressure. It is hard to say how much the hydrogen concentration really drops because it can not be measured during the reaction and after the reaction, there is a completely different equilibrium due to the lower pressure and temperature when the reactor is cooled down. This problem would require additional research to answer properly.

Hydrogen influence on reaction rate

The reaction order for hydrogen was found to be 0.332 and the influence of the amount of hydrogen and its reaction order can be seen in figure 5.8. Hydrogen speeds the reaction up slightly until about five minutes after which its concentration decreases as discussed above. In the end, the reaction speed is decreased by roughly a third. This seems plausible even though other research has often assumed the reaction order for hydrogen to be zero because of a suspected overabundance of hydrogen [9, 12, 19]. Through various iterations of the model, the reaction order for hydrogen ranged from 0.28 to 0.44 so its exact value is not precise.

5.4 Mass transfer limitations

The mass transfer resistances that were included in this research are the evaporation rate and the internal diffusion resistances inside the catalyst. The other mass transport limitations will also be discussed. Finally, an explanation for the rate-limiting step will be given.

Evaporation
The volumetric evaporation rates can be seen in table 5.1. The density was obtained at the boiling point of each compound and at 60 bars pressure as explained in section 3.4. The density increases with size, which is to be expected but appears to stay constant or go down even for the largest compounds, which is most likely because the boiling point decreases faster than the increase in density.
The molar volume, however, clearly increases with size as the molecular weight increases. The subsequent liquid diffusion ratio between the compounds is highest for the smaller compounds. This can be explained by the fact that smaller compounds can easier diffuse through a liquid with less resistance from other molecules.

Table 5.1: Volumetric evaporation rate for all compounds which are assumed to evaporate and values from which it is calculated

Compound name	C1	C2	C3	C4	C5	C6	C7	C8	C9	C10	C11	C12	C13	H2
Density $[kg/m^3]$	428	549	587	609	618	622	624	623	620	617	599	609	605	76.9
Molar volume $[m^3/mole]$	0.037	0.055	0.075	0.095	0.12	0.14	0.16	0.18	0.21	0.23	0.26	0.28	0.30	0.026
Diffusion ratio	1	0.88	0.79	0.73	0.68	0.65	0.61	0.59	0.56	0.54	0.52	0.51	0.50	1.1
Volumetric evaporation $[m^3/s]$ (10^{-9})	15.4	13.6	12.2	11.3	10.5	10.0	9.47	9.06	8.70	8.38	8.04	7.86	7.63	17.4

Bin Jumah et al. (2021) found that the gas compounds (C1-C4) evaporate on average 1.4 times as fast as naphtha (C5-C12) [9]. In these results, C3 evaporates 1.35 times faster compared to C8 which brings it in line with the literature results. The mass transfer coefficients could not be compared because the hollow stirrer used in experiments creates a larger than normal gas-liquid surface area. The mass transfer coefficient is simply an arbitrary parameter which makes the pressure profile match the experimental results. As discussed in section 5.3, the evaporation rate for hydrogen is most likely larger than as calculated because it is the only viable explanation for the difference in pressure profile and the residual hydrogen after the reaction. It could be caused by the difference in the way that it evaporates because the hydrocarbons mostly evaporate while hydrogen mostly dissolves. It could also be caused because Raoult's law does not take into account vapour phase imperfections. More research needs to be done to accurately predict the evaporation rate of hydrogen. The evaporation rates for the hydrocarbons seem to be accurate.

Catalyst effectivity
The Thiele modulus for every hydrocarbon gives the ratio of the maximum conversion rate in the catalyst particle to the maximum diffusion transport rate and can be seen in figure 5.9.

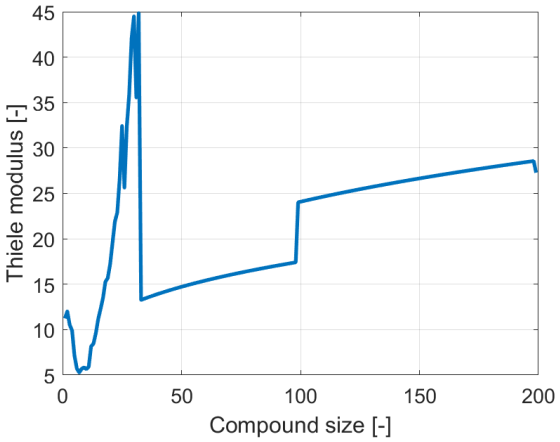

Figure 5.9: Modelled Thiele modulus for all hydrocarbons

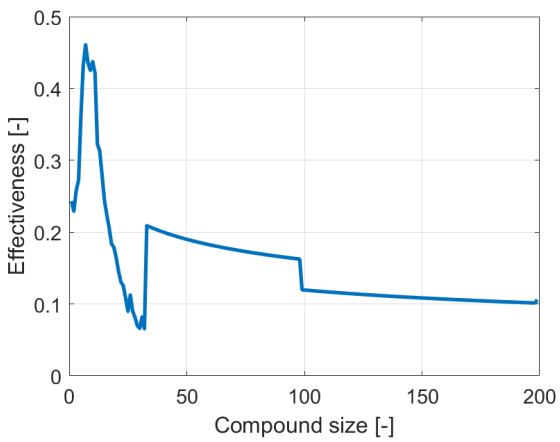

Figure 5.10: Modelled effectiveness factor for all hydrocarbons

Because the Thiele modulus is above one for every compound, the rate-limiting step within the catalyst is clearly the diffusion rate when Knudsen diffusion is dominant. The diffusion rate is most limiting for the biggest compounds because the Thiele modulus increases with the fourth root of the molecular weight ($\phi \sim MW^{1/4}$). The reaction rate distribution has a great influence over the Thiele modulus distribution. This is because the reaction rates greatly vary as will be discussed in more detail in section C.3 of the appendix.

The effectiveness is the ratio of the actual volume averaged reaction rate to the rate of reaction if the internal surface area was entirely exposed to the bulk liquid concentration, it can be seen in figure 5.10. Since it is calculated from the Thiele modulus only it roughly has its inverted shape. The polymer is only able to use the catalyst with 11% effectiveness.

Bin Jumah et al. (2021) found an effectiveness of 82% and used non-linear regression to obtain this value. A catalyst was used with a pore entrance diameter of 12 T atoms which is almost 30 times as small as assumed in this thesis. It should be said that the catalyst properties for this thesis were unavailable for the experimental results so values were taken from the literature as described in chapter 4.

Seitz et al. (2022) found an effectiveness of 20% when using 1.8 mm particles at 673 K and calculated this by dividing the measured reaction rate of the catalyst by the reaction rate of a powder sample [40]. The latter would have very few internal diffusion limitations because of its minuscule size. When comparing with the results of Seitz et al. (2022), it is likely that the effectivity for the experiment in this thesis would be a lot higher than 20% because smaller particles are assumed and at lower temperatures.

Fuentes-Ordóñez et al. (2013) mostly tested the effectiveness at higher temperatures and higher molecular weight but when extrapolating the result, an effectiveness of at least 50% would be expected for the used temperature and molecular weight [14]. Fuentes-Ordóñez et al. (2013) calculated this using multiple advanced methods for determining the molecular diffusion and used the initial reaction rate and polymer concentration within a solvent. This makes it difficult to replicate for this thesis because multiple advanced methods were used which could not have been completed in the given time frame.

In this thesis, Knudsen diffusivity is assumed to be dominant because that was also used in the kinetics and catalysis course [24] of CSE-b. Because the above-named papers indicate that the effectivity would be higher for the used temperature, molecular weight, and catalyst characteristics it is concluded that Knudsen diffusivity is likely not dominating the molecular diffusion within the catalyst.

We can assess the validity of the Knudsen diffusion by looking at the average pore diameter of the catalyst, which is 30 nm. While the size of an LDPE molecule is 26.8 nm in its length when a C-C total bond length of 1.45 angstroms is used [41]. This implies that the polymer will only fit within the pore on its side and will experience resistance which limits the diffusion within the catalyst. Nevertheless, this is only true when the polymer enters the catalyst pore on its side which means that in practice, more interaction will happen between molecules instead of between molecules and the catalyst.
It can be said that, because of this, Knudsen diffusion will not be dominant for the polymer inside the catalyst. Calculating the exact molecular diffusion could not be done within the given time, given its complexity. For the other hydrocarbons the effectivity was also calculated by Knudsen diffusion as a simplification, but it is unlikely that for smaller compounds Knudsen diffusion will be more limiting than normal molecular diffusion.

The calculated Knudsen diffusion (m^2/s) can be compared with literature molecular diffusion rates from the work of Yuan et al. (2021) [42]. Calculations were done using equations 3.9, 3.10, and 3.11 from section 3.4.2 and can be seen in table 5.2. The literature values are based on an MFI zeolite (silicalite-1) catalyst. The article has a pore size of $6 \cdot 10^{-10} m$ but does not mention catalyst size, porosity, or tortuosity so it is difficult to compare. It is assumed that these values are the same as the values chosen in this thesis. The results show that the calculated Knudsen diffusion is roughly ten times as slow as the molecular diffusion measured in the article. This means that the effectiveness of the catalyst is roughly a factor of three lower compared to these measured diffusion rates. This implies that the real effectiveness is quite a bit higher in reality, closer to the aforementioned literature values.

Finally, it should be mentioned that in other research the influence of the hydrogen concentration was not taken into account and when this is added to the reaction equation, the reaction constant has to increase by 20 to 50 times in order to result in the same hydrogenolysis rate when hydrogen was not part of the reaction equation. This has greatly influenced the final effectiveness as can be seen in table 5.2 which is on average 60% higher. This is closer to the values from the aforementioned literature. In the future, it will be necessary to calculate the effectiveness factor without relying on the presence of hydrogen in the hydrogenolysis equation. This can be done by using $1/s/mole^m$ as the units for the kinetic rate constants instead of $1/s$.

Table 5.2: Modelled Knudsen diffusion and effectiveness compared to literature [42] with pore size $6{\cdot}10^{-10}m$

Compound	C4	C8	C12
Modelled Knudsen diffusion (m^2/s)	$3.2 \cdot 10^{-10}$	$2.3 \cdot 10^{-10}$	$1.9 \cdot 10^{-10}$
Literature molecular diffusion (m^2/s)	$3.0 \cdot 10^{-9}$	$2.5 \cdot 10^{-9}$	$2.1 \cdot 10^{-9}$
Effectiveness from model	0.043	0.084	0.076
Effectiveness calculated from literature	0.12	0.25	0.23
Effectiveness model without hydrogen	0.071	0.14	0.12
Effectiveness literature without hydrogen	0.22	0.38	0.28

In conclusion, it can be said that the effectiveness is likely to be higher than 11% and that Knudsen diffusion is likely not the dominant diffusion within the catalyst. An accurate result can be obtained when the characteristics of the catalyst were known, a more exact calculation for the molecular diffusion were done, and the kinetic rate constant units were changed for the calculations. Please note that the calculated effectiveness should not be considered an exact value. Rather, based on specific assumptions, it should be viewed as a conclusion that can assist in future modelling efforts. The inaccuracy of the modelled effectivity will not impact the other results because the lower effectivity is offset by an increased kinetic reaction rate. More information on the kinetic cracking rate can be found in appendix C.3.

Other mass transport limitations

It was assumed earlier that gas and liquid phase concentration gradients and external liquid-solid diffusion were not the rate-limiting steps in this process. It is safe to disregard the gas concentration gradient as the starting molar fraction is one and only decreases to 0.54 by the end of the reaction, as shown in figure C.15 of the appendix section C.5. This indicates that the gas is not significantly diluted. In addition, the gasses have relatively high diffusion rates. Therefore, it can be said that no concentration gradient within the gas phase will limit the reaction speed as is also assumed in literature [9, 14].

A liquid concentration gradient can be neglected because it is calculated that $1.9 \cdot 10^6$ catalyst particles were used in the reaction, based on the assumed density and porosity. This number is possibly inflated because the chosen catalyst characteristics are chosen from different sources. Nonetheless, there are likely enough catalyst particles in the liquid dispersed to decrease the effective distance from the liquid bulk to the catalyst surface. This implies that a liquid concentration gradient will likely not limit the reaction rate too much as is also assumed in literature [9, 14], but more research is needed.

The external diffusion limitation as done by Fuentes-Ordóñez et al. (2013) [14] is quite difficult to calculate and would only have been possible if more time was available. It can, however, be assumed safely that the external diffusion limitation is not the rate-limiting step. This is because, when extrapolating with the used reaction conditions in the work of Fuentes-Ordóñez et al. (2013) [14], the external diffusion limitation is relatively small. The experimental conditions used in this thesis have a lower temperature, higher stirring rate, lower molecular weight, lower pressure, and a lower particle size. All of these parameters mean that the external diffusion limitation is very low for the used experimental conditions but more research is needed to say with greater accuracy for this specific reaction.

Rate-limiting step

It is not possible to predict the rate-limiting step in this process with the given information. This is because the three most probable candidates are most likely not correctly predicted by the model. Literature is also divided on which part is the rate-limiting step. Fuentes-Ordóñez et al. (2013) [14] has found that the internal diffusion limitation (effectiveness) is the rate-limiting step while Bin Jumah et al. (2021) [9] claims it is the hydrogenolysis reaction itself, specifically the hydrogenolysis of polyolefins into heavy liquid. How the rate-limiting step would have been calculated, if more information would have been available, is discussed in the appendix section C.4.

Chapter 6

Statistics

About the fit

The fit can be examined by plotting the experimental data against the same points in the model. This can be seen in figure 6.1. On the left side of the dotted line, the model over-predicts the experimental values and on the right side of the line, the model under-predicts the experimental results. The fit appears to be good since all the values are distributed relatively close to the line. The pressure is a little bit higher compared to the data and the residual hydrogen has one good and one bad data point which has been discussed above. The yield has both good and bad fits. The fit for the values at 21 minutes is worse because the regression favours the first and final data point usually.

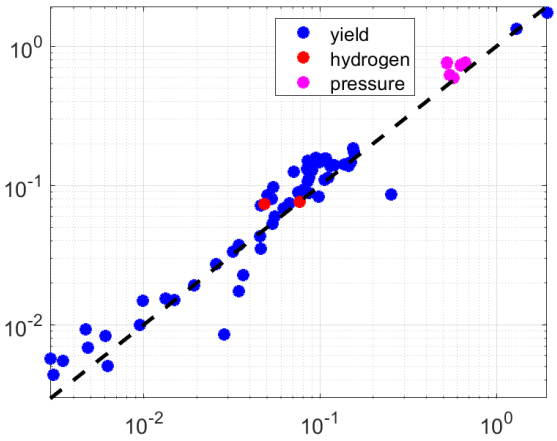

Figure 6.1: Experimental data against modelled data over a 45-degree line

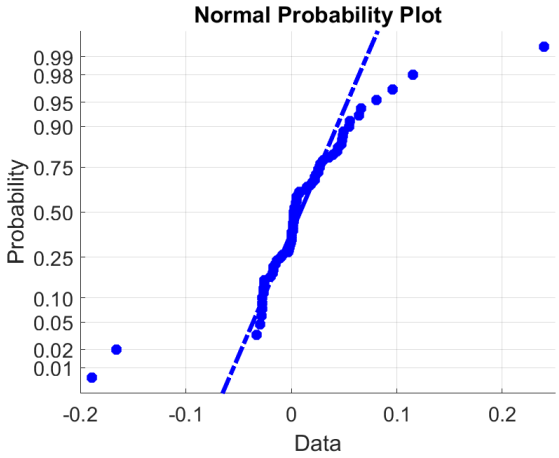

Figure 6.2: Modelled residuals normal probability

On average the model seems to overpredict more often. This is most likely because the yield of the experimental results is low for some smaller compounds and because the evaporation rate of hydrogen is likely higher in reality as discussed before. The largest errors in the model seem to come from the under-predicting of the yield of various larger compounds at 21 minutes. More data points are needed to say more about the fit. With more data points, the most likely result is that the model will more accurately predict the yield over time instead of just the final yield. This would require the larger compounds to have a higher kinetic rate constant so their yield can decrease faster over time as can be seen in figure 5.1.

The residual normal probability can be seen in figure 6.2. If the plot is linear or has a small S shape, the errors are normally distributed over the fitted values [43]. It can clearly be seen that this criteria is met for most of the residuals but there are a few outliers. The outlying residuals have already been discussed.

Analysis of variance

The analysis of the variance table can be seen in table 6.1. The degrees of freedom are such because there are 75 data points and 37 parameters. It should be mentioned that the sum of squares is not calculated logarithmically. This implies that the influence of the pressure on the results is much larger compared to the yield and residual hydrogen because it is magnitudes larger. This can mostly be seen in the sum of squares due to the regression which is dominated by the pressure. The pressure was divided by ten to limit this influence a little bit but if time would have permitted this could better have been calculated logarithmically from the start.

Table 6.1: Modelled analysis of variance table (ANOVA)

ANOVA	Degrees of freedom	Sum of squares	Mean square
Regression	36	166.8	4.63
Residuals	38	0.197	0.0052
Total	74	166.99	

The sum of squares and the mean square of the residuals are relatively low because the fit appears to be good and there are a lot more data points as compared to the parameters.

Changes to the initial guess of the parameters did not improve the fit as can be seen in table 6.2 where it shows that every change increased the total sum of squares. Therefore, it can be concluded that the right initial guess values were chosen.

Table 6.2: Modelled total sum of squares for multiple parameters guess changes. No change means a guess for the kinetic rate constant=$0.05s^{-1}$, volumetric evaporation rate=$2 \cdot 10^{-8}$, and hydrogen reaction order=0.4

Parameter guess change	Amount	Total sum of squares
No change		166.99
Kinetic rate constant	0.01 s^{-1}	167.3
Kinetic rate constant	0.1 s^{-1}	167.1
Volumetric evaporation rate	$3 \cdot 10^{-8} m^3/s$	175.5
Volumetric evaporation rate	$1 \cdot 10^{-8} m^3/s$	175.5
Hydrogen reaction order	0.5	167.2
Hydrogen reaction order	0.3	168.8

Other tests
An f-test for the regression could not be done because the non-linear equation does not have an independent constant term. Non-linear regression also does not allow R^2 to be calculated. The lack of fit and confidence intervals could also not have been done because the measurements were not repeated. The plot of the residuals against the fitted values can be seen in figure D.1 of the appendix section C.5 but no conclusions could be drawn from it because of the variation in magnitudes.

Correlation matrix
Finally, a correlation matrix between the used parameters was made. The entire table can be seen in figure D.2 of the appendix section C.5. It is unfortunately very hard to find a pattern in the matrix and Matlab gives a warning that the matrix is close to singular or badly scaled which might result in inaccurate results. It can be said that the evaporation rate and the hydrogen reaction order scale positively to each other. This implies that if one increases, it would cause the other to also increase. This can be explained by the fact that if more hydrogen dissolves into the liquid phase, the concentration increases which means that the reaction order can be higher because it does not have to slow the reaction speed down due to a great lack of hydrogen. It can also be seen that an increase in the reaction rate of C2 to C5 has a positive effect on each other because the extra mass that is formed must quickly be reacted away to keep the yield low of this group.

Chapter 7

Conclusion

The research goal was to find out how the experimental results of the hydrogenolysis of plastic can be predicted by a kinetic model when using non-linear regression in Matlab. The kinetic model considers changes in density, volume, and compressibility and is based on the experimental results from the hydrogenolytic cracking of LDPE on a Ru/C catalyst. The results show that the model can mostly predict the experimental results based on the assumptions made. The residuals are, for the most part, evenly distributed. This means that the research goal has been achieved.

Based on least square fitting, it was found that the kinetic rate constants for the formation of alkanes range between 0.0140 and 0.504 s^{-1}. The volumetric evaporation rate for methane is 15.40 m^3/s and the hydrogen reaction order is 0.332. The mean square of the regression and residuals was found to be 4.63 and 0.0052 respectively, indicating a good fit. The conversion of the polymer is most likely above 97% but could not be calculated accurately. The model has given a greater inside into the chemistry inside of the hydrogenolysis of LDPE, getting us one small step closer to a more sustainable world.

Two issues are found which prevent getting the best fit: inaccurate experimentally measured yield and a faulty described hydrogen evaporation process. Firstly, the experimental yield is probably underpredicting the yield of C4 to C6 and C27 to C33. The yield predicted by the model for C1 to C33 is probably more accurate than the experimental values, specifically for the aforementioned carbon ranges. Secondly, the evaporation process for hydrogen is likely not connected to the evaporation rates of the hydrocarbons based on the liquid diffusion ratio between the compounds.

Some other assumptions will also need changing. The rate-limiting step in the process could unfortunately not be determined due to a lack of catalyst information. The catalyst's internal diffusion is likely higher than calculated, and Knudsen diffusion is not dominant. Literature suggests the effectiveness factor is higher than calculated under these reaction conditions. However, the lower effectiveness did not make the overall fit worse because this was offset by a higher kinetic rate constant, meaning that the results are useful. In the current model, each compound till C33 has its own kinetic rate constant, this makes it easier for the regression to offset some of the faults in the model but in the future, fewer fitting parameters would have to be used for more scientific certainty.

The other assumptions made do not seem to impact the results in any negative way.

Chapter 8

Future improvements

Experimental
Firstly, a different method for measuring the experimental yield is needed. This caused the yield of some of the smaller compounds to be underestimated which greatly reduced the accuracy of the model which is reflected in the pressure and the residual hydrogen.

Secondly, the characteristics of the catalyst are greatly needed for accurate calculations of the catalyst's effectiveness.

Also, to get a better final fit more data points in time would be greatly helpful in getting more accurate kinetic rate constants. Dual measurements can also lead to a better statistical certainty of the results.

Mass transfer resistance calculations
The evaporation of hydrogen was linked to the evaporation of hydrocarbons in this model based on the diffusion rates of the liquids. This caused the hydrogen concentration in the liquid to decrease which is not supported by literature or expectation. This implies that a different method for the evaporation of hydrogen would be required. This is unfortunately very difficult to do given the type of stirrer used which gives an unpredictable gas-liquid surface area.
The calculation of the Hatta number could be used instead for the liquid-gas mass transport processes or could give a greater inside into the mass transfer resistance.

Also, the effectiveness of the catalyst was said to be controlled by Knudsen diffusion. This was likely incorrect because more interaction happens between molecules compared to interaction between molecules and the catalyst pore surfaces. A better calculation for the internal diffusion would be required. The effectivity was calculated using a rate constant which did not take hydrogen into account and used incorrect units. Therefore, a modified equation is needed instead. The chemical reaction reacts in series which could also be taken into account.

The liquid-solid interface was assumed to not be the rate-limiting step based on a comparison between the used reaction conditions and literature findings. This was done because of a lack of catalyst information and the limited amount of time available for this thesis.

Calculations can also be done to check for concentration gradients in the gas and liquid phases. This is not likely to greatly affect the reaction but it would be very interesting to compare the resistances between every part of the mass transfer process and the reaction rate to determine the rate-limiting step of the process.

Assumptions and other
The hydrogenolysis mechanism does not take into account branched products, selectivity to crack a molecule at a certain place, catalyst deactivation, density changes affecting the reaction rate, a different reaction order, and temperature gradients. This could be added to the model for greater accuracy.

Some other assumptions like taking only C200 as the feed, calculating the density only at 60 bar, and calculating the compressibility for only two components could also be changed for greater accuracy.

Changing the reaction conditions like temperature, catalyst size, amount of catalyst, hydrogen pressure, and feed composition, would also make the model more dynamic towards predicting the yield under different conditions. The catalyst ratio to feed would be linear if no mass transport limitations emerge. Using different temperatures would also allow for the calculation of the activation energy with the Arrhenius equation.

The financial side of the process could be explored by calculating the required energy which is the difference in enthalpy between the feed and the end product.

Calculating the Lewis number, which is the local heat of reaction, can also give greater inside.

Finally, calculating the sum of squares logarithmically to limit the influence of a difference in parameter magnitude. It would also help to use fewer parameters when fitting against the experimental data. The mean square error can be used to track how much a parameter improves the fit.

Chapter 9

Symbols

symbol or abbreviation	name	unit
a	Attraction parameter	$m^3 J/mol^2$
A,B,C,D,E	Vapour pressure fitting parameters	-
b	Repulsion parameter	m^3/mol
$C_{i,G}$	Concentration hydrocarbon i gas phase	mol/m^3
C_{H_2}	Concentration hydrogen in liquid	mol/m^3
C_i^*	Gas-liquid interface concentration compound i	mol/m^3
C2	Hydrocarbon with two carbon atoms (ethane)	-
C-C	Carbon-carbon covalent bond	-
C-H	Carbon-Hydrogen covalent bond	-
CSE-b	Chemical science and engineering bachelor UT	-
$D_{eff,i}$	Effective diffusion constant hydrocarbon i in liquid	m^2/s
$D_{K,i}$	Knudsen diffusion constant hydrocarbon i in liquid	m^2/s
$D_{M,i}$	Molecular diffusion constant hydrocarbon i in liquid	m^2/s
D_i	Liquid diffusion i constant	m^2/s
d_p	Diameter catalyst pore	m
Da	Molecular weight amount	g/mol
DP_i	Degree of polymerisation hydrocarbon (length i)	-
GC	Gas chromatography	-
GC-MS	Gas chromatography coupled with mass spectroscopy	-
GPC	Gel permeation chromatography	-
H_i	Henry constant compound i	Pa
i	Length of hydrocarbon i	-
j	Length of hydrocarbon j	-

symbol or abbreviation	name	unit
k	Simplification term acentric factor	-
$k_{i,j}$	Binary interaction parameter between i and j	-
$k_{i,tot}$	Total kinetic rate constant hydrocarbon i	1/s
k_i	Cracking kinetic rate constant single bond	1/s
K_i	Total hydrogenolysis rate hydrocarbon i	mol/s
K_i^c	Cracking rate hydrocarbon i	mol/s
K_i^f	Formation rate hydrocarbon i	mol/s
$k_L a_i$	Volumetric evaporation rate compound i	1/s
LDPE	Low density polyethylene	-
m	Reaction order hydrogen	-
$M_{w,i}$	Molecular weight hydrocarbon i	g/mol
m_c	Mass of all catalyst particles	kg
m_i	Mass hydrocarbon i	kg
MW	Molecular weight	g/mol
$n_{H_2}^m$	Amount hydrogen and reaction order m	mole
$n_{i,G}$	Amount hydrocarbon i gas phase	mol
$n_{i,L}$	Hydrocarbon i amount in liquid	mol
P	Total pressure	Pa
P_c	Critical pressure	Pa
P_i^*	Vapour pressure i	Pa
R	Gas constant	J/mol/K
$R_{K,i}$	Cracking rate of single bond	mol/s
R_c	Radius of catalyst particle	m
rpm	Rate per minute	-
Ru	Ruthenium	-
Ru/C	Ruthenium on carbon support	-
t	Time	s
T	Temperature	K
T_c	Critical temperature	K
T_r	Reduced (relative) temperature	K
$V_{i,mol}$	Molar volume solute i	m^3/mol
$V_{solv,mol}$	Molar volume solvent	m^3/mol

symbol or abbreviation	name	unit
V_{total}	Total reactor volume	m^3
V_G	Gas phase volume	m^3
V_L	Liquid phase volume	m^3
V_m	Molar volume	m^3/mol
w	Acentric factor	-
x_i	Mole fraction i in liquid	-
y_i	Mole fraction i in gas	-
Z	Compressibility factor	-
z_i	Mole fraction i	-
α	Acentric component	K
ρ_c	Density catalyst (activated carbon)	kg/m^3
ρ_i	Density hydrocarbon i	kg/m^3
η	Effectiveness hydrocarbon i	-
π	Pi	-
ϵ	Porosity	-
ϕ_i	Thiele modulus hydrocarbon i	-
τ	Tortuosity	-
ρ	Total density	kg/m^3
η_{solv}	Viscosity of solvent	Pa s

List of Figures

List of Tables

Bibliography

[1] Philip J. Landrigan, Hervé Raps, and Maureen Cropper. "The Minderoo-Monaco Commission on Plastics and Human Health". In: *Annals of Global Health* 89.1 (Mar. 2023), pp. 23–24. ISSN: 2214-9996. DOI: 10.5334/AOGH.4056. URL: https://annalsofglobalhealth.org/articles/10.5334/aogh.4056.

[2] Niyitanga Evode, Sarmad Ahmad Qamar, and Muhammad Bilal. "Plastic waste and its management strategies for environmental sustainability". In: *Case Studies in Chemical and Environmental Engineering* 4 (Dec. 2021), p. 100142. ISSN: 2666-0164. DOI: 10.1016/J.CSCEE.2021.100142.

[3] Giorgia Guglielmi. "In the next 30 years, we'll make four times more plastic waste than we ever have". In: *Science* (July 2017). ISSN: 0036-8075. DOI: 10.1126/SCIENCE.AAN7121.

[4] OECD. *Global Plastics Outlook*. OECD, Feb. 2022. DOI: 10.1787/DE747AEF-EN. URL: https://www.oecd-ilibrary.org/environment/global-plastics-outlook_de747aef-en.

[5] *Plastic packaging waste: 38% recycled in 2020 - Products Eurostat News - Eurostat*. URL: https://ec.europa.eu/eurostat/web/products-eurostat-news/-/ddn-20221020-1.

[6] Kim Ragaert, Laurens Delva, and Kevin Van Geem. "Mechanical and chemical recycling of solid plastic waste". In: *Waste Management* 69 (Nov. 2017), pp. 24–58. ISSN: 0956-053X. DOI: 10.1016/J.WASMAN.2017.07.044.

[7] Christopher Igwe Idumah and Iheoma C. Nwuzor. "Novel trends in plastic waste management". In: *SN Applied Sciences* 1.11 (Nov. 2019), pp. 1–14. ISSN: 25233971. DOI: 10.1007/S42452-019-1468-2/FIGURES/12. URL: https://link.springer.com/article/10.1007/s42452-019-1468-2.

[8] R. Miandad et al. "Catalytic pyrolysis of plastic waste: A review". In: *Process Safety and Environmental Protection* 102 (July 2016), pp. 822–838. ISSN: 0957-5820. DOI: 10.1016/J.PSEP.2016.06.022.

[9] Abdulrahman Bin Jumah et al. "Kinetic Modeling of Hydrocracking of Low-Density Polyethylene in a Batch Reactor". In: *ACS Sustainable Chemistry and Engineering* 9.49 (Dec. 2021), pp. 16757–16769. ISSN: 21680485. DOI: 10.1021/ACSSUSCHEMENG.1C06231/ASSET/IMAGES/LARGE/SC1C06231{_}0013.JPEG. URL: https://pubs.acs.org/doi/full/10.1021/acssuschemeng.1c06231.

[10] Linxiao Chen, Yifeng Zhu, and Laura C. Meyer. "Effect of reaction conditions on the hydrogenolysis of polypropylene and polyethylene into gas and liquid alkanes". In: *Reaction Chemistry & Engineering* 7.4 (Mar. 2022), pp. 844–854. ISSN: 2058-9883. DOI: 10.1039/D1RE00431J. URL: https://pubs.rsc.org/en/content/articlehtml/2022/re/d1re00431j%20https://pubs.rsc.org/en/content/articlelanding/2022/re/d1re00431j.

[11] Pavel A. Kots, Sibao Liu, and Brandon C. Vance. "Polypropylene Plastic Waste Conversion to Lubricants over Ru/TiO2Catalysts". In: *ACS Catalysis* 11 (2021), pp. 8104–8115. ISSN: 21555435. DOI: 10.1021/ACSCATAL.1C00874/SUPPL{_}FILE/CS1C00874{_}SI{_}001.PDF. URL: https://pubs.acs.org/doi/abs/10.1021/acscatal.1c00874.

[12] Yosuke Nakaji, Masazumi Tamura, and Shuhei Miyaoka. "Low-temperature catalytic upgrading of waste polyolefinic plastics into liquid fuels and waxes". In: *Applied Catalysis B: Environmental* 285 (May 2021), p. 119805. ISSN: 0926-3373. DOI: 10.1016/J.APCATB.2020.119805.

[13] J. Aguado, D. P. Serrano, and J. M. Escola. "Fuels from waste plastics by thermal and catalytic processes: A review". In: *Industrial and Engineering Chemistry Research* 47.21 (Nov. 2008), pp. 7982–7992. ISSN: 08885885. DOI: 10.1021/IE800393W/ASSET/IMAGES/LARGE/IE-2008-00393W{_}0001.JPEG. URL: https://pubs.acs.org/doi/full/10.1021/ie800393w.

[14] Edwin G. Fuentes-Ordóñez et al. "Transport phenomena in catalytic hydrocracking of polystyrene in solution". In: *Industrial and Engineering Chemistry Research* 52.42 (Oct. 2013), pp. 14798–14807. ISSN: 15205045. DOI: 10.1021/IE401968R/ASSET/IMAGES/LARGE/IE-2013-01968R{_}0011.JPEG. URL: https://pubs.acs.org/doi/full/10.1021/ie401968r.

[15] P S Marathe, R J M Westerhof, and S R A Kersten. "Fast pyrolysis of lignins with different molecular weight: Experiments and modelling". In: *Applied Energy* 236 (2019), pp. 1125–1137. ISSN: 0306-2619. DOI: https://doi.org/10.1016/j.apenergy.2018.12.058. URL: https://www.sciencedirect.com/science/article/pii/S0306261918318750.

[16] Pushkar Satish Marathe. "The interplay between chemistry and transport phenomena during the fast pyrolysis of cellulose, lignin and biomass". PhD thesis. Enschede, The Netherlands: University of Twente, Sept. 2019. ISBN: 9789036548458. DOI: 10.3990/1.9789036548458. URL: https://research.utwente.nl/en/publications/the-interplay-between-chemistry-and-transport-phenomena-during-th.

[17] *Mechanical Recycling – European Bioplastics e.V.* July 2020. URL: https://www.european-bioplastics.org/mechanical-recycling/.

[18] Yoshinao Nakagawa, Shin Ichi Oya, and Daisuke Kanno. "Regioselectivity and Reaction Mechanism of Ru-Catalyzed Hydrogenolysis of Squalane and Model Alkanes". In: *ChemSusChem* 10.1 (Jan. 2017), pp. 189–198. ISSN: 1864-564X. DOI: 10.1002/CSSC.201601204. URL: https://onlinelibrary.wiley.com/doi/full/10.1002/cssc.201601204%20https://onlinelibrary.wiley.com/doi/abs/10.1002/cssc.201601204%20https://chemistry-europe.onlinelibrary.wiley.com/doi/10.1002/cssc.201601204.

[19] Yosuke Nakaji et al. "Regioselective hydrogenolysis of alga-derived squalane over silica-supported ruthenium-vanadium catalyst". In: *Fuel Processing Technology* 176 (July 2018), pp. 249–257. ISSN: 0378-3820. DOI: 10.1016/J.FUPROC.2018.03.038.

[20] S. L. Wong, T. A. Tuan Abdullah, and N. Ngadi. "Parametric study on catalytic cracking of LDPE to liquid fuel over ZSM-5 zeolite". In: *Energy Conversion and Management* 122 (Aug. 2016), pp. 428–438. ISSN: 0196-8904. DOI: 10.1016/J.ENCONMAN.2016.06.009.

[21] NICE CXone Expert. *1.9: Diffusion - Chemistry LibreTexts*. URL: https://chem.libretexts.org/Bookshelves/Inorganic_Chemistry/Introduction_to_Solid_State_Chemistry/01%3A_Lectures/1.09%3A_Diffusion.

[22] Shaofen Li. "Chemical Reaction and Transport Phenomena in Heterogeneous System". In: *Chemical Reaction Engineering* (2017), pp. 265–310. DOI: 10.1016/B978-0-12-410416-7.00006-9.

[23] Shijie Liu. "Mass Transfer Effects". In: *Bioprocess Engineering* (2017), pp. 949–1005. DOI: 10.1016/B978-0-444-63783-3.00016-2.

[24] L. Lefferts. *Kinetics and catalysis course*. 2021.

[25] Jianwei Li and Peter W. Carr. "Accuracy of Empirical Correlations for Estimating Diffusion Coefficients in Aqueous Organic Mixtures". In: *Analytical Chemistry* 69.13 (July 1997), pp. 2530–2536. ISSN: 00032700. DOI: 10.1021/AC961005A/ASSET/IMAGES/MEDIUM/AC961005AE00015.GIF. URL: https://pubs.acs.org/doi/full/10.1021/ac961005a.

[26] Divya Gootam et al. "Modeling Growth Kinetics of Methane Hydrate in Stirred Tank Batch Reactors". In: *ACS Engineering Au* 1.2 (Dec. 2021), pp. 148–159. ISSN: 2694-2488. DOI: 10.1021/ACSENGINEERINGAU.1C00012. URL: https://pubs.acs.org/doi/full/10.1021/acsengineeringau.1c00012.

[27] NICE CXone Expert. *5: Equation of State - Engineering LibreTexts*. URL: https://eng.libretexts.org/Bookshelves/Chemical_Engineering/Distillation_Science_(Coleman)/05%3A_Equation_of_State.

[28] Seif Eddeen K. Fateen, Menna M. Khalil, and Ahmed O. Elnabawy. "Semi-empirical correlation for binary interaction parameters of the Peng-Robinson equation of state with the van der Waals mixing rules for the prediction of high-pressure vapor-liquid equilibrium". In: *Journal of Advanced Research* 4.2 (Mar. 2013), pp. 137–145. ISSN: 20901232. DOI: 10.1016/J.JARE.2012.03.004. URL: http://demonstrations.wolfram.com/PengRobinsonEquationOfStateForMixtures/.

[29] *Ruthenium on carbon extent of labeling: 5 wt. % loading — Sigma-Aldrich*. URL: https://www.sigmaaldrich.com/NL/en/product/aldrich/206180.

[30] Rasyid Syidiq et al. "Characterization of Activated Charcoal Oil Palm (Elaeis Guineensiss Jacq) Shell Waste using SEM and FTIR: Effect of Activation Temperature". In: *Indonesian Review of Physics* 2.2 (Dec. 2019), p. 67. ISSN: 2621-3761. DOI: 10.12928/IRIP.V2I2.812.

[31] *L.van der Ham (used for catalyst assumption)*. 2023.

[32] *Carbon, Activated - Materials Handled - Flexicon Corporation*. URL: https://www.flexicon.com/Materials-Handled/Carbon-Activated.html.

[33] *NIST/TRC Web Thermo Tables (WTT): Critically Evaluated Thermophysical Property Data*. 2012. URL: https://wtt-pro.nist.gov/wtt-pro/.

[34] C. L. Yaws. *Chemical Properties Handbook (online)*. McGraw-Hill Education, 1999. Chap. 11. ISBN: 9780070734012. URL: https://www.accessengineeringlibrary.com/content/book/9780070734012%20https://www.accessengineeringlibrary.com/content/book/9780070734012.abstract.

[35] *The Properties of Gases & Liquids, 4th Edition (R. C. Reid, J. M. Prausnitz & B. E. Poling) — Tamm Hdz - Academia.edu*. URL: https://www.academia.edu/33161453/The_Properties_of_Gases_and_Liquids_4th_Edition_R_C_Reid_J_M_Prausnitz_and_B_E_Poling_.

[36] *Polyolefins, Plastics Europe*. URL: https://plasticseurope.org/plastics-explained/a-large-family/polyolefins/.

[37] *Relative tolerance for solver tolerance calculation - MATLAB - MathWorks Benelux*. URL: https://nl.mathworks.com/help/simulink/gui/relativetolerance.html.

[38] *Solve nonlinear curve-fitting (data-fitting) problems in least-squares sense - MATLAB lsqcurvefit - MathWorks Benelux*. URL: https://nl.mathworks.com/help/optim/ug/lsqcurvefit.html.

[39] *Hydrogen Compressibility at different temperatures and pressures — Hydrogen Tools*. URL: https://h2tools.org/hyarc/hydrogen-data/hydrogen-compressibility-different-temperatures-and-pressures.

[40] Mathias Seitz and Stephan Schröter. "Catalytic Depolymerization of Polyolefinic Plastic Waste". In: *Chemie Ingenieur Technik* 94.5 (May 2022), pp. 720–726. ISSN: 1522-2640. DOI: 10.1002/CITE.202100182. URL: https://onlinelibrary.wiley.com/doi/full/10.1002/cite.202100182%20https://onlinelibrary.wiley.com/doi/abs/10.1002/cite.202100182%20https://onlinelibrary.wiley.com/doi/10.1002/cite.202100182.

[41] John D. Roberts and Marjorie C. Caserio. *Bond Lengths and Double-Bond Character*. URL: https://chem.libretexts.org/Bookshelves/Organic_Chemistry/Basic_Principles_of_Organic_Chemistry_(Roberts_and_Caserio)/21%3A_Resonance_and_Molecular_Orbital_Methods/21.09%3A_Bond_Lengths_and_Double-Bond_Character.

[42] Jiamin Yuan, Zhiqiang Liu, and Yimo Wu. "Thermal resistance effect on anomalous diffusion of molecules under confinement". In: *Proceedings of the National Academy of Sciences of the United States of America* 118.21 (May 2021), p. 2102097118. ISSN: 10916490. DOI: 10.1073/PNAS.2102097118/-/DCSUPPLEMENTAL. URL: /pmc/articles/PMC8166051/%20/pmc/articles/PMC8166051/?report=abstract%20https://www.ncbi.nlm.nih.gov/pmc/articles/PMC8166051/.

[43] *4.6 - Normal Probability Plot of Residuals — STAT 501*. URL: https://online.stat.psu.edu/stat501/lesson/4/4.6.

[44] MargaretO Ilomuanya et al. "Effect of pore size and morphology of activated charcoal prepared from midribs of Elaeis guineensis on adsorption of poisons using metronidazole and Escherichia coli O157:H7 as a case study". In: *Journal of Microscopy and Ultrastructure* 5.1 (Mar. 2017), pp. 32–38. ISSN: 2213-879X. DOI: 10.1016/J.JMAU.2016.05.001.

[45] J. Wei. "Least Square Fitting of an Elephant". In: *CHEMTECH* 5.2 (1975), pp. 128–129. URL: https://demonstrations.wolfram.com/FittingAnElephant/.

Appendix A

Theory

A.1 Different hydrogenolysis reaction mechanism

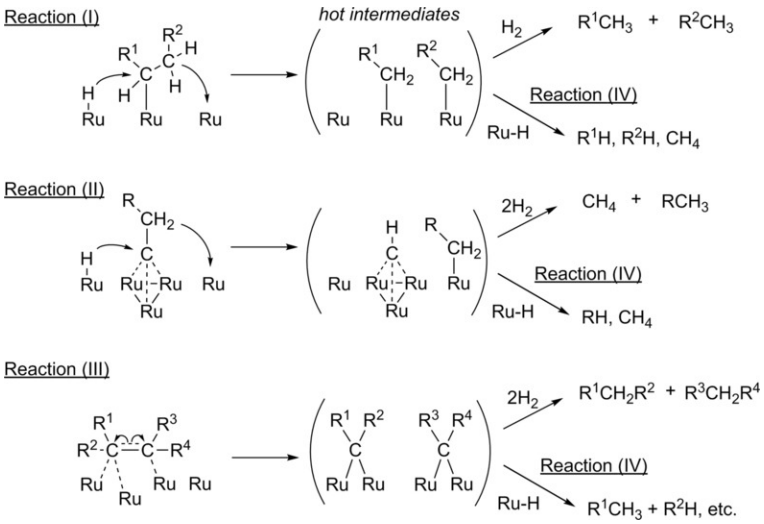

Figure A.1: Reaction mechanism on catalyst for different products [18]

The hydrocarbons crack into different kinds of alkanes. It can crack into two linear carbon chains, loose carbons (methane), and branched products, see figure A.1. Reaction (I) is the reaction that can also be seen in figure 3.1 and is the main reaction in the process. Reaction (II) describes the formation of methane when a single carbon bond breaks from the carbon chain. Reaction (III) is a reaction with branched hydrocarbons. Within this thesis, it is assumed that no branched products exist for simplification of the kinetic model. This is supported by the experimental data which shows almost no branching of the reaction products. Reaction (IV) describes a second hydrogenation process where different products can be created.

A.2 Differential equations

The equations from all the sections in this chapter come together to describe the change in the amount of hydrocarbons and hydrogen in the liquid and gas phases. The complete rate equation for hydrocarbons in the liquid phase can be seen in equation A.1.

$$\frac{\mathrm{d}n_{i,L}}{\mathrm{d}t} = 2 \cdot \left(\sum_{j=i+1}^{i_{max}} \frac{k_{j,tot} \cdot n_{j,L} \cdot {n_{H_2,L}}^m \cdot \eta_j}{j-1} \right) - k_{i,tot} \cdot n_{i,L} \cdot {n_{H_2,L}}^m \cdot \eta_i - k_L a_i \cdot (C_i^* - C_i) \qquad \text{(A.1)}$$

The formation part is a function of the total kinetic rate constant (s^{-1}), amount (mole), hydrogen amount and reaction order (mole), and the effectivity (-) as calculated above for all compounds which are larger than i. The effectivity is a function of temperature, molecular weight, catalyst pore diameter, tortuosity, porosity, catalyst radius, the total kinetic rate constant, catalyst total mass, catalyst density, hydrogen concentration, and hydrogen reaction order.
It should be said that this is purely a mathematical description of the formation part and that it is disputed whether the hydrogen amount actually plays a role in this reaction. The process of hydrogenolysis shares

the same parameters as the formation process but is comparatively simpler. Finally, the last part is the evaporation to the gas phase. This can be seen in equation A.2.

$$\frac{\mathrm{d}n_{i,G}}{\mathrm{d}t} = k_L a_i \cdot (C_i^* - C_i) \tag{A.2}$$

The evaporation rate is based on the volumetric evaporation constant (m^3/s), the concentration at the gas-liquid interface ($mole/m^3$), and the bulk concentration in the gas phase ($mole/m^3$).
The evaporation rate for compound i is connected to the other evaporation rates based on the molecular weight and the density at the boiling point.
The bulk concentration is calculated with the volume of the gas phase (m^3) which depends on the reactor volume, the density, and the composition of the liquid phase.
The interface concentration is calculated with the vapour pressure, mole fraction in the liquid phase, temperature and compressibility. The vapour pressure is calculated based on a specific relation with temperature. The compressibility is calculated with the critical temperature and pressure, and the binary interaction parameter for the two assumed components. The reduced temperature is also needed.
The equation counts for both the hydrogen and the hydrocarbons from the perspective of the gas phase. The hydrogen in the liquid phase is a function of the evaporation (dissolving) of hydrogen from the gas phase and the total hydrogenolysis rate of all hydrocarbons. This can be seen in equation A.3.

$$\frac{\mathrm{d}n_{H_2,L}}{\mathrm{d}t} = -\sum_{n=2}^{n_{max}} (k_{i,tot} \cdot n_{i,L} \cdot {n_{H_2,L}}^m \cdot \eta_i) - k_L a_{H2} \cdot (C_{H_2}^* - C_{H2}) \tag{A.3}$$

Appendix B

Method

B.1 Experimental process and measurements

The catalyst chosen in this process is Ruthenium because it shows good reactivity and selectivity and the support is activated carbon because it has a great internal surface area and relatively low cost. Activated carbon can have micro-pores as small as 2 nm in width [44] and macro-pores as large as 50 nm. It is assumed that there is no coke formation or deactivation of the catalyst during the reaction which is supported by experimental results. There is no solvent added to the polymer and it is assumed to contain no branches.

The reactor is placed under 40.1 bar pure hydrogen pressure from a hydrogen storage vessel to start the hydrogenolysis process and to avoid the formation of double bonds. In the beginning, the assumed gas phase consists of 0.118 grams of pure hydrogen. The reactor is quickly heated to 523 Kelvin by lowering it in a pre-heated fluidized sand bed with a pneumatic arm and is kept at this temperature during the reaction time. It is assumed that there is no temperature gradient within the reactor. A hollow-shaft mechanical stirrer stirs the liquid and sucks the hydrogen into the liquid mixture. At the melting point of the used plastic, the stirrer is put on $\sim$ 700 rpm and switched to $\sim$ 1300 rpm when the operating temperature is reached. At this temperature, the pressure increased to around 65 bars.

When the process is finished, the reactor is quickly cooled down by submerging it in the cooling bath to stop the reaction. The pressure decrease in the hydrogen vessel can be assumed to be the consumed hydrogen. Cooling the reactor down causes the gas-liquid equilibrium to change dramatically. The smallest six components are assumed to occupy the gas phase at this lower temperature and pressure and are analysed by gas chromatography (GC). Compounds of range C5 to C33, which are assumed to be the liquid product, are analysed with gas chromatography coupled with mass spectrometry (GC-MS) and gel permeation chromatography (GPC) for the molecular weight distribution.

B.2 Model description

Pre-calculations
The first part of the model consists of the pre-calculations that go into the model like reaction conditions, physical properties and the experimental data, see section 4.1. The rules for the model like tolerance, boundaries for the parameters, and parameter guess values are also required. To prevent the regression from seeking extreme values and achieving a mathematical fit that is not supported by literature [9], the kinetic rate constants must fall within the range of 1 to 10^{-4} which are the boundary values.

Regression
The second part consists of the regression itself and calls a function in which the modelled results are interpolated to fit against the experimental values at the correct points in time. The values from the model are converted to mass and the values for C34-C200 are added together for comparison with the experimental data. The gas and liquid parts of the model are added up because the measurements are done at lower pressure and temperatures which means the phase compositions will have changed significantly. This is why a total yield is used in the form of weight distribution. The pressure is calculated at five points in time and is also compared to the experimental data. Since there are two data points in time each with 35 compounds (one for hydrogen) and five data points for the pressure there are a total of 75 experimental values that are used for the fit. This part takes by far the longest for the model to calculate, with 436 seconds when using the mentioned settings.

Differential equations
The third part is the function with the differential equations describing the reaction and all other calculations that are required for it. It is called upon by both the regression and the eventual plotting of the

results. It calculates the hydrogenolysis rate, evaporation rate, effectivity, density, liquid diffusion ratio, volumes, compressibility, and vapour pressure. This can be seen in chapter 3.

The output of the model is the change in amount of moles over time for 200 liquid components, 13 gaseous components and hydrogen for both the liquid and gas phase which gives 215 in total. The model calculates 38 minutes of reaction time which is equal to the longest experiment and consists of 1001 time steps.

Post-calculation
The fourth and final part of the model consists of generating the results from the function and doing mass checks and statistical analysis like the sum of squares and mean squares of the regression, a correlation matrix between the parameters, plotting the fitted values against the data, plotting the residuals normal probability, and plotting the residuals against the fitted values. The largest part of the model in terms of length of code is plotting the results in various ways as can be seen in the results (chapters 5) and the appendix.

B.3 Figures

$$Gas\ yield = Y_G = \frac{mass\ of\ C_x\ in\ product}{mass\ fed\ polyolefin} \times 100\%\ (with\ x = 1\ -\ 4) \qquad \text{Eq. 1}$$

$$Naphtha\ yield\ = Y_N = \frac{mass\ of\ C_x\ in\ product}{mass\ fed\ polyolefin} \times 100\%\ (with\ x = 5\ -\ 11) \qquad \text{Eq. 2}$$

$$Liquid\ yield = Y_L = \frac{mass\ of\ C_x\ in\ product}{mass\ fed\ polyolefin} \times 100\%\ (with\ x = 12\ -\ 33) \qquad \text{Eq. 3}$$

$$Wax\ yield\ = Y_W = \frac{mass\ product - mass\ catalyst\ - quantified\ mass}{mass\ fed\ polyolefin} \times 100\% \qquad \text{Eq. 4}$$

$$Mass\ balance\ closure = MBC = \frac{mass\ product}{mass\ fed\ polyolefin + mass\ catalyst} \times 100\% \qquad \text{Eq. 5}$$

Figure B.1: Yield equations for experimental data

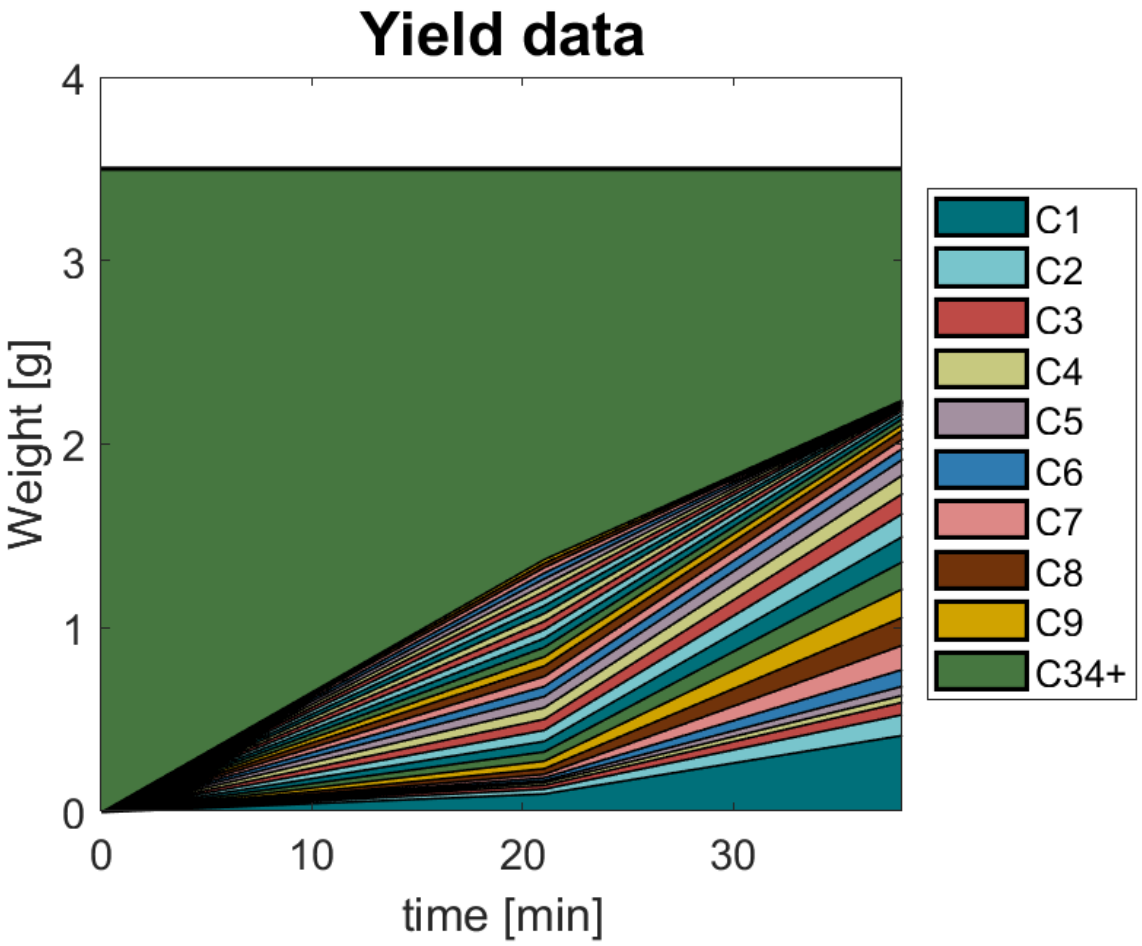

Figure B.2: Experimental mass evolution over time

Appendix C

Discussion and results

C.1 Phase composition

The products in the liquid phase of the process can be seen in figure C.1. C200, which represents the polymer, decreases quickly in yield to the point where it is one of the lowest yields. The other large compounds like C100 and C150 increase quickly at first because they have a large molecular weight but then also decrease quickly as they react away and there are fewer and fewer even larger compounds which can increase their yield. The smaller components increase more slowly because of their smaller molecular weight but keep rising because there are more than enough larger compounds remaining. After 20 minutes the formation of these compounds slows down because there are not as much larger compounds remaining and the hydrogen concentration decreases by this point as will be described in section 5.3. The largest mass quantity of any component in the liquid phase by the end is C10, due to the evaporation of methane, but in terms of mole quantity, it is still methane.

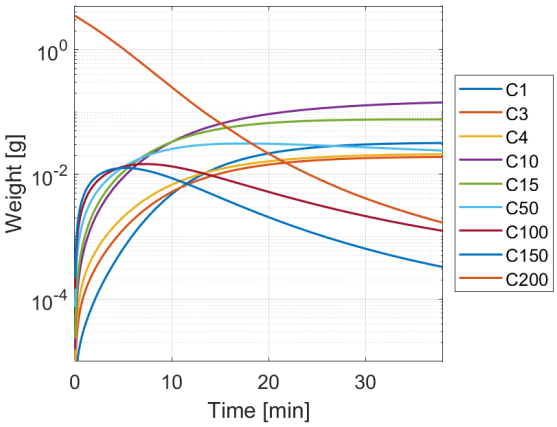

Figure C.1: Modelled liquid phase mass for some compounds over time

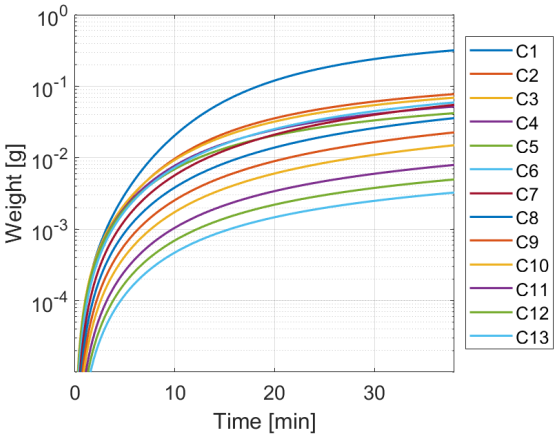

Figure C.2: Modelled gas phase mass for hydrocarbons which are assumed to evaporate over time

The products in the gas phase of the process can be seen in figure C.2. The separation between the compounds can be seen very clearly and can be explained by the decrease in vapour pressure with increased size (see figure 4.3) and the decreasing mass transfer component (see section 5.4, table 5.1). Methane is also more often formed than some of the others which creates the gap between methane and the next compound. There is ten times as much methane in the gas phase as in the liquid phase in the end. There is about forty times as much C13 in the liquid phase as in the gas phase, supporting the assumption that compounds larger than C13 barely evaporate.
The liquid and gas products in moles can be seen in figures C.10 and C.11 in the appendix.

C.2 Conversion

The yield in mass percentage for some compounds over time can be seen in appendix figure C.9. The conversion of the polymer for multiple kinetic rate constants can be seen in table C.1. It can be seen that lowering the kinetic rate guess to 0.005 slightly decreased the conversion. An even lower kinetic rate guess most likely made the regression give up on trying to approximate the guess, this resulted in a slightly higher conversion. It can therefore be said that the conversion of the polymer could not be accurately calculated but is most likely above 97%. This matches with the experimental results which show a lower

viscosity than most polyolefins, pointing to a high polyolefin conversion.

Table C.1: Modelled conversion of polymer for multiple kinetic rate constants

Kinetic rate constant guess	Kinetic rate constant modelled	Conversion
0.05	0.085	99.85%
0.005	0.035	96.08%
0.0005	0.040	96.70%

C.3 Hydrogenolysis rate

Modelled kinetic rate constants

The total kinetic rate constants $k_{i,tot}$ can be seen in figure C.3. The rate constant start at C2 because that is the smallest compound that is able to crack. The rates for C2 to C5 are relatively high because the yield of these products is lower compared to some others. As is explained in sections 5.1 and 5.3, the yield for C4 to C6 products is likely to be higher than what is measured because the measurement equipment has more difficulty in measuring this group. That being said, it is also possible that these compounds are small enough to react further within the smallest pores of the catalyst, which causes the rates of these compounds to increase which the effectivity is unable to predict.

Compounds C6 to C17 have lower rates than average because they have relatively higher yields. This can be explained because these compounds are perhaps not small enough to react deep within the catalyst pores but are also not large enough to adsorb on the catalyst, resulting in a lower-than-average hydrogenolysis rate.

Compounds C18 to C33 have relatively higher rate constants. This could be caused by a greater adsorption bond with the catalyst sites or by the fact that larger compounds 'bounce' into the catalyst pores more often due to their larger size. Larger compounds have a higher molecular weight which reduces the Knudsen diffusion as calculated with equation 3.10. It is also possible that the issue could be attributed to challenges with the measuring equipment as discussed earlier. This means that the groups C27 to C33 should have a higher yield and that the yield of C34+ would subsequently be smaller. This would result in lower rate constants for the C27 to C33 group.

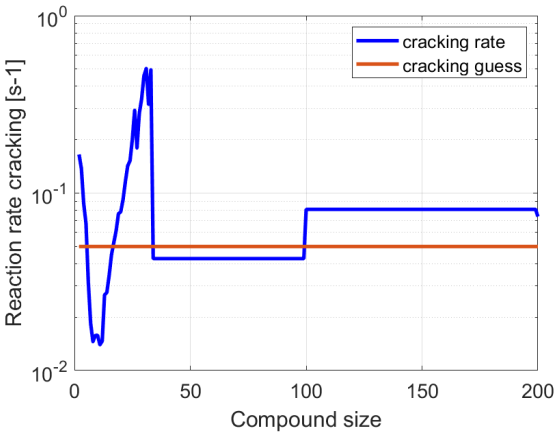

Figure C.3: Modelled kinetic rate constants and kinetic rate constant guess for all hydrocarbons

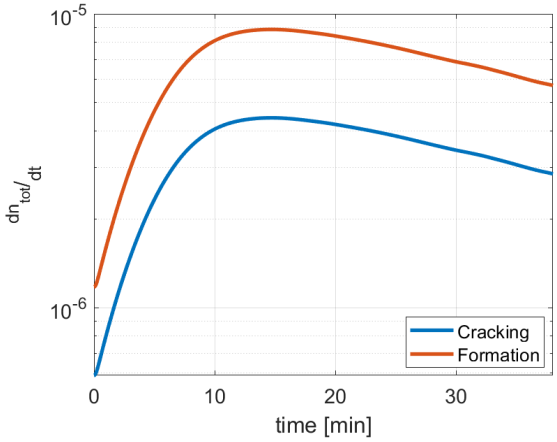

Figure C.4: Modelled total hydrogenolysis and formation rates over time

The reaction rates for C34 to C99 are grouped together as one value to make the regression faster and to use fewer parameters. If too many parameters are used then it is theoretically possible to 'fit an elephant' [45] which means that any data set can be fitted if the model has enough options to do it with. Because this group has no experimentally-defined, quantitative yield, it is hard to say if the hydrogenolysis rate is accurate. It is a lot lower than the rates for C17 to C33 which could indicate that the reaction rate for those compounds is too high. It could also mean that at a certain size, the diffusion within the catalyst becomes too difficult which lowers the reaction rate.

The reaction rates for the compounds C100 to C199 are also grouped together and give a higher rate than the previous group. This is not in line with what was previously said, which was that groups larger

than C33 react slower because their size makes diffusion more difficult. This implies that either the regression has inaccurately predicted the reaction rate for C100 to C199 or it is more proof that the yield for some compounds is underestimated by the measuring equipment. The most likely answer is a combination of both explanations.
The reaction rate of the polymer (assumed to be C200) is roughly on par with that of the previous group.

Throughout various iterations of the model, the reaction rate constants for the compounds larger than C33 are very sensitive to the initial rate constant guess and the upper and lower boundaries. This implies that their results have low certainty.

When calculating the reaction rate constants with the influence of hydrogen, the resulting reaction rates are significantly higher, ranging from 20 to 50 times, compared to those obtained without hydrogen. Due to a lack of time, the kinetic rate constant was calculated with units $1/s$ instead of $1/s/mole^m$ for simplification. This implies that the kinetic rate constants can not be compared to other research because they often do not include hydrogen which they assume to be zero order [9, 12].

It should be said that the cracking and formation rates are more based on mathematics than on actual chemical details. For instance, the cracking rate is most likely not relative to the hydrogen concentration because the alkane cracks with the hydrogen molecules that are formed when that alkane bonds with the catalyst surface. This can be seen in figure 3.1 in section 3.2.
The hydrogenolysis mechanism was chosen because it allowed for a constant mass over time which is important for the accuracy of the model. In the future, this can also be done by building a model which checks, at each step, if the total mass is still constant and keeps trying until it achieves that result.

Total hydrogenolysis rate
The total cracking and formation rates can be seen in figure C.4 and the cracking and formation rates for multiple components separately can be seen in figures C.16 and C.17 in the appendix. The total formation rate is always twice as large as the cracking rate because two compounds are always formed out of one. The reaction starts slowly as there is only C200 in large supply which has only a small amount of moles to react. As the amount of moles increases over the course of the reaction, there are simply more compounds that can crack as compared to the beginning. This can be seen in figure C.5 in the appendix. After ten minutes the reaction starts to slow down as the concentration of hydrogen decreases.

At the end of the process, the reaction rate is slowed down by a third because of a lower hydrogen concentration as can be seen in figure 5.8. The reaction is also slowed down because there is relatively more methane which does not crack and because some compounds have evaporated into the gas phase where they can not make contact with the catalyst. The latter appears to have the largest effect on ethane which appears almost five times as much in the gas phase as in the liquid phase.

The compounds smaller than C6 have a higher amount in the gas phase than in the liquid phase by the end of the reaction. This implies that evaporation has a great effect on the reaction rate for these smaller compounds. This matches with the fact that compounds smaller than C6 are also over their boiling point at 523 K and 60 bar [33]. The smaller compounds have a higher evaporation rate than a dissolving rate because their amount in the gas phase only grows over time, even though it does slow down.
An attempt was made to calculate the rate constants as a function of their size in order to use fewer parameters for the regression and to make a more mathematical distribution for the reaction rates instead of individual values. This could unfortunately not be done in the given time but an attempt to fit the calculated rate constants over ten different parameters can be seen in appendix figure C.18, equation C.2 and table C.2. The largest problem when fitting the rate constants is the group C18 to C33, providing more evidence that the yield of this group is greatly underestimated.

C.4 Rate-determining step

The evaporation of hydrogen should be much higher to avoid a significant decrease in the hydrogen concentration. The effectiveness of the catalyst should also be higher since it will likely not be dominated by Knudsen diffusion. The kinetic rate constants should be lower because the model overpredicts them to make up for the lower effectivity. Therefore, it can be concluded that the rate-limiting step is dependent on the exact reaction conditions. Specifically, the temperature, catalyst characteristics, and polyolefin molecular weight significantly influence the mass transport limitations. This could unfortunately not be done because of a lack of catalyst information. More research into this topic will be needed.

If more information should have been available about the catalyst and a correct evaporation rate for hydrogen was used, the rate-limiting step would be determined by looking at the greatest mass transport

resistance. This can for example be calculated with equation C.1.

$$J_A a = \frac{C_{A,G}}{\frac{1}{k_G} + \frac{1}{k_L a} + \frac{1}{m k_{LS} a_S} + \frac{1}{m k_1^n s_S}} \tag{C.1}$$

Here, $J_A a$ is the overall transfer rate from the gas phase ($mole/m^3/s$), $C_{A,G}$ is the concentration of A in the gas phase ($mole/m^3$), and the other terms represent the mass transfer rates for each part of the mass transport process and the total hydrogenolysis rate (s^{-1}).

C.5 Figures

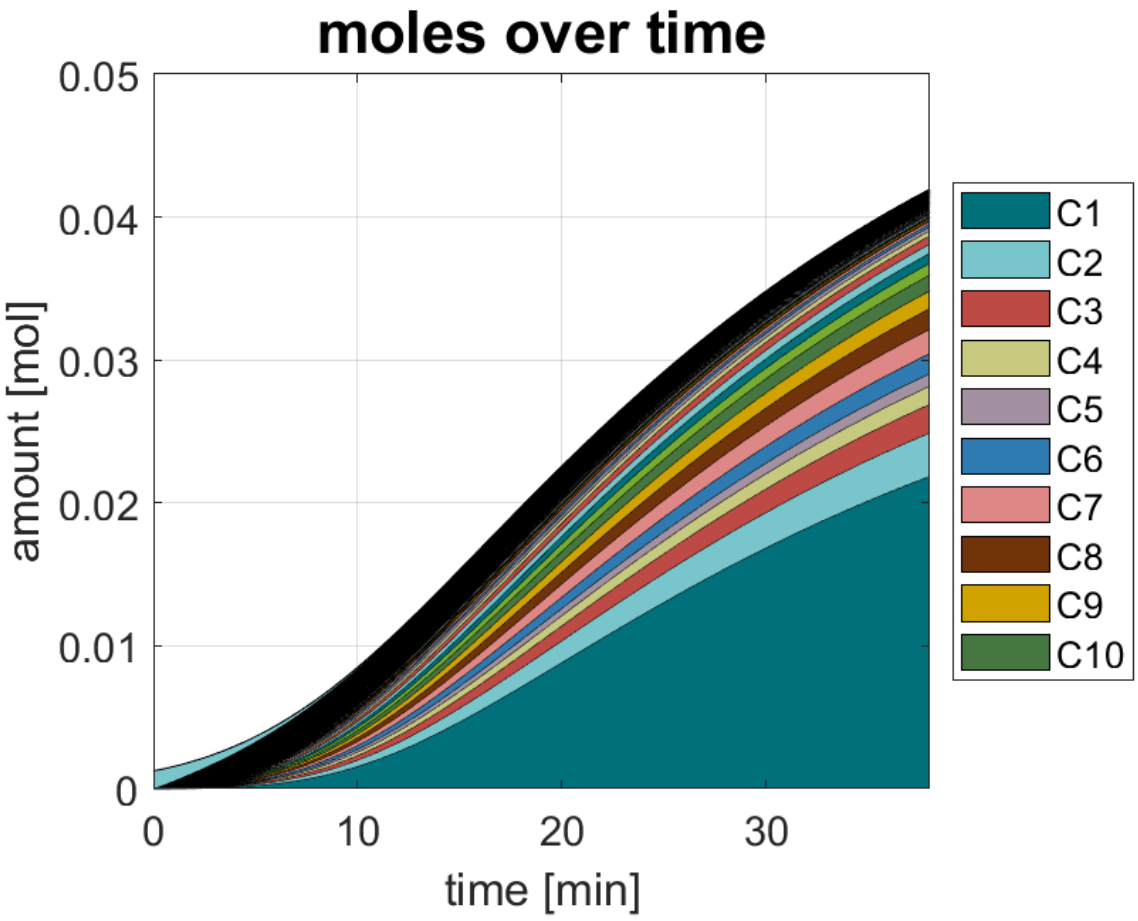

Figure C.5: Modelled amount in moles for hydrocarbons over time

Table C.2: Modelled kinetic rate constant fit parameters

A	B	C	D	E	F	G	H	I	J
-1.37	-0.0061	2.95	-1.37	0.0042	4.07e-4	0.8405	$1.65 \cdot 10^{-4}$	$-1.79 \cdot 10^{-6}$	$2.98 \cdot 10^{-9}$

$$k(n) = A + B \cdot n + \frac{C}{n} + D \cdot n^E + F \cdot (n - 50)^2 + G \cdot ln(n) + H^n + I \cdot n^3 + J \cdot n^4 \tag{C.2}$$

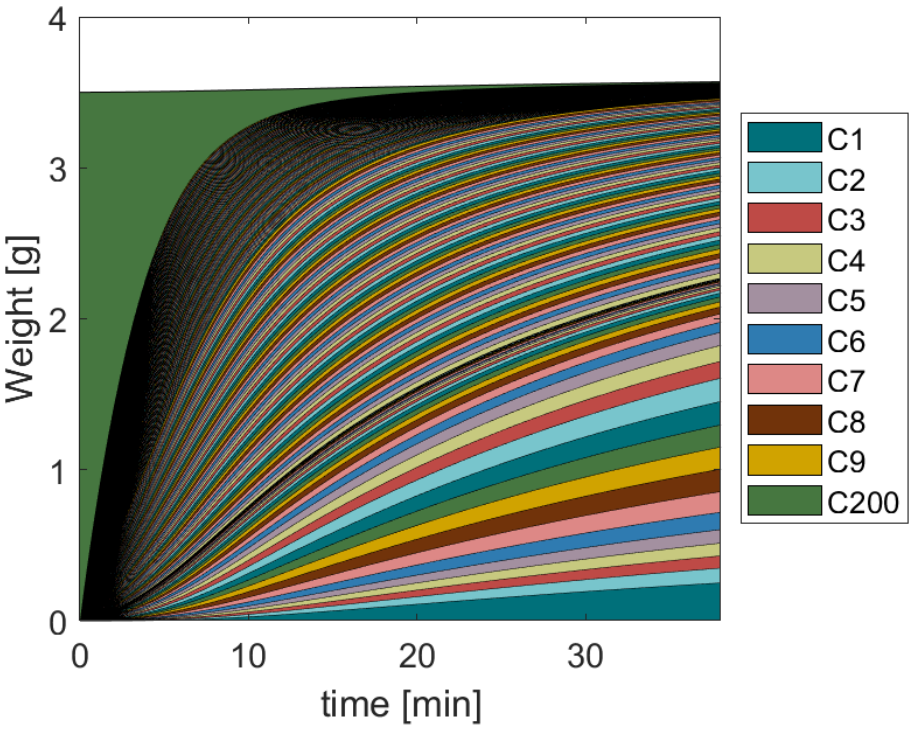

Figure C.6: Modelled evolution of mass of hydrocarbons over time (detailed)

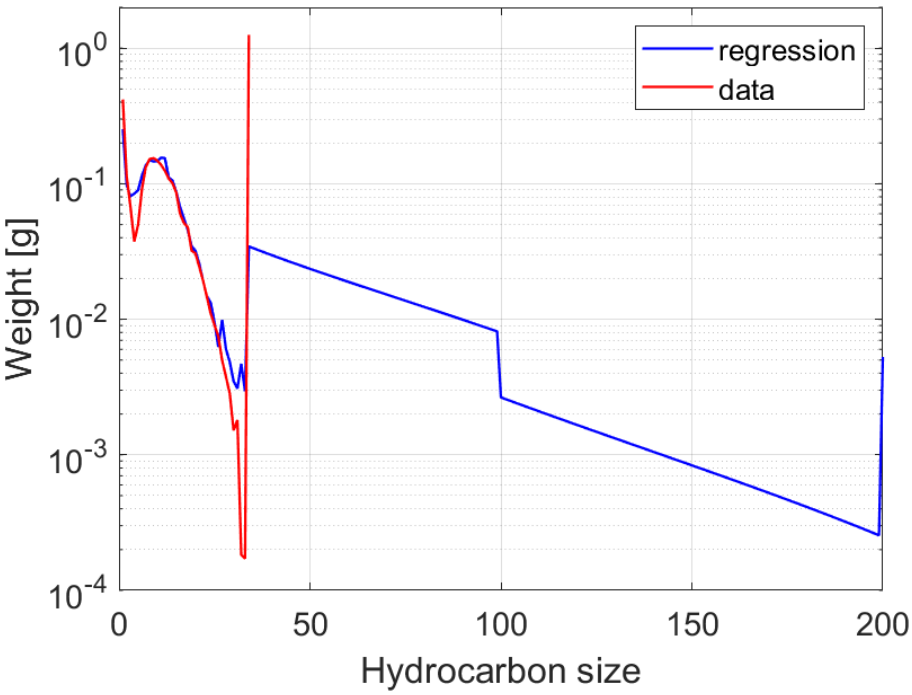

Figure C.7: Modelled mass of hydrocarbons against experimental data

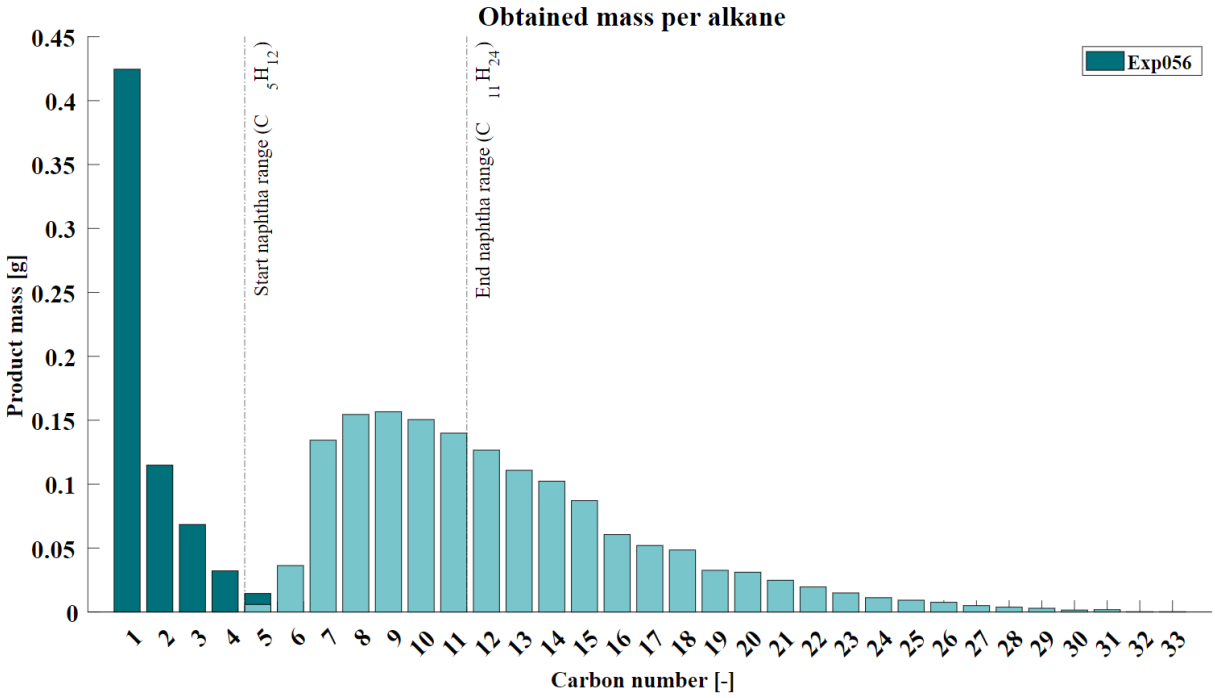

Figure C.8: Experimental measurement mass overlap from GC and GC-MS

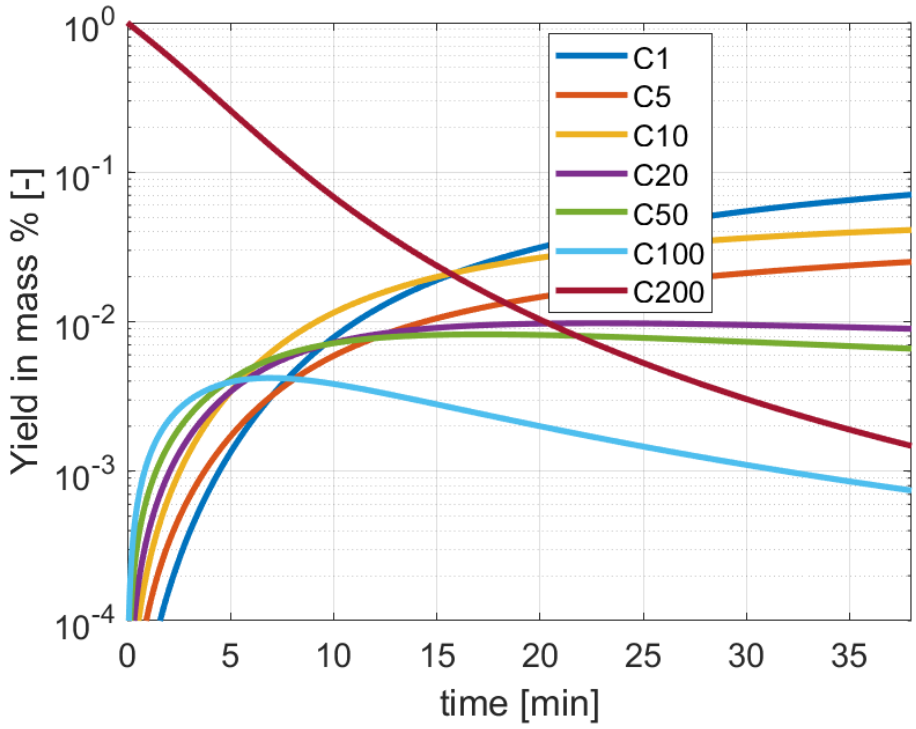

Figure C.9: Modelled yield in mass fraction of selected compounds over time

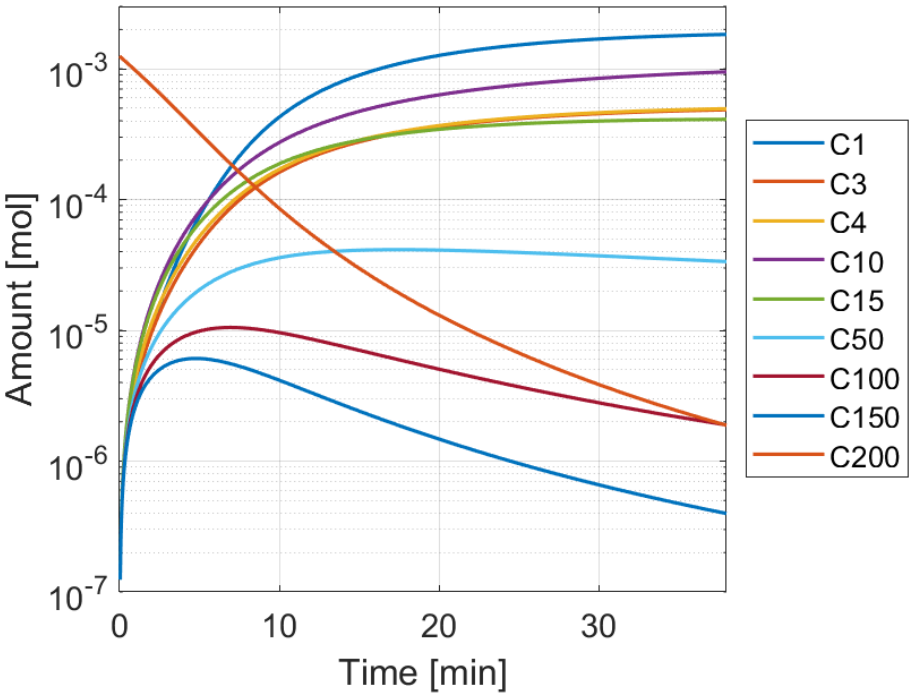

Figure C.10: Modelled liquid phase of some compounds in moles over time

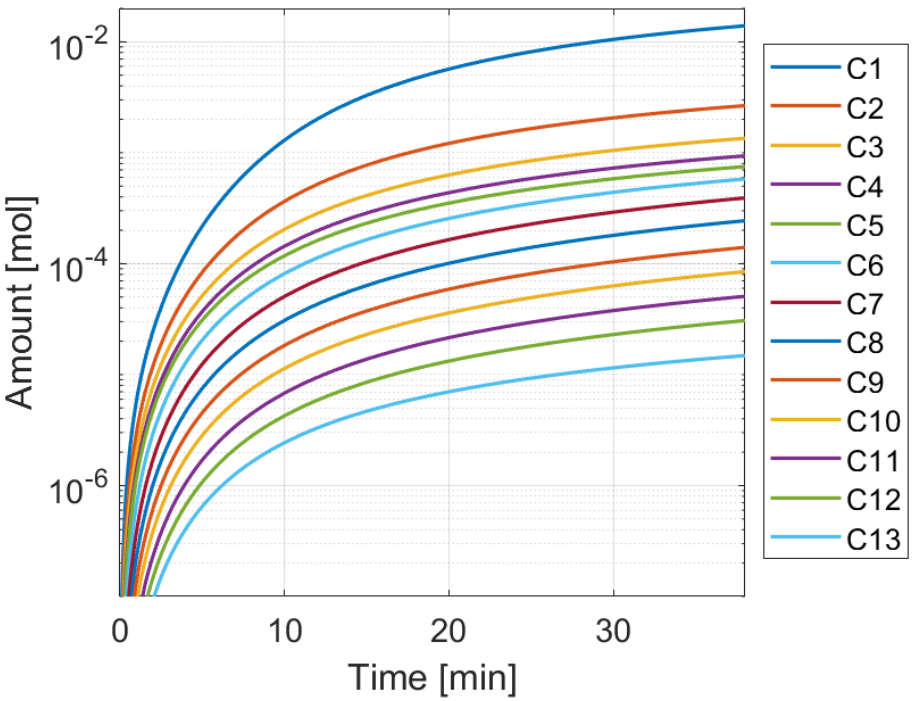

Figure C.11: Modelled gas phase for evaporating hydrocarbon in moles over time

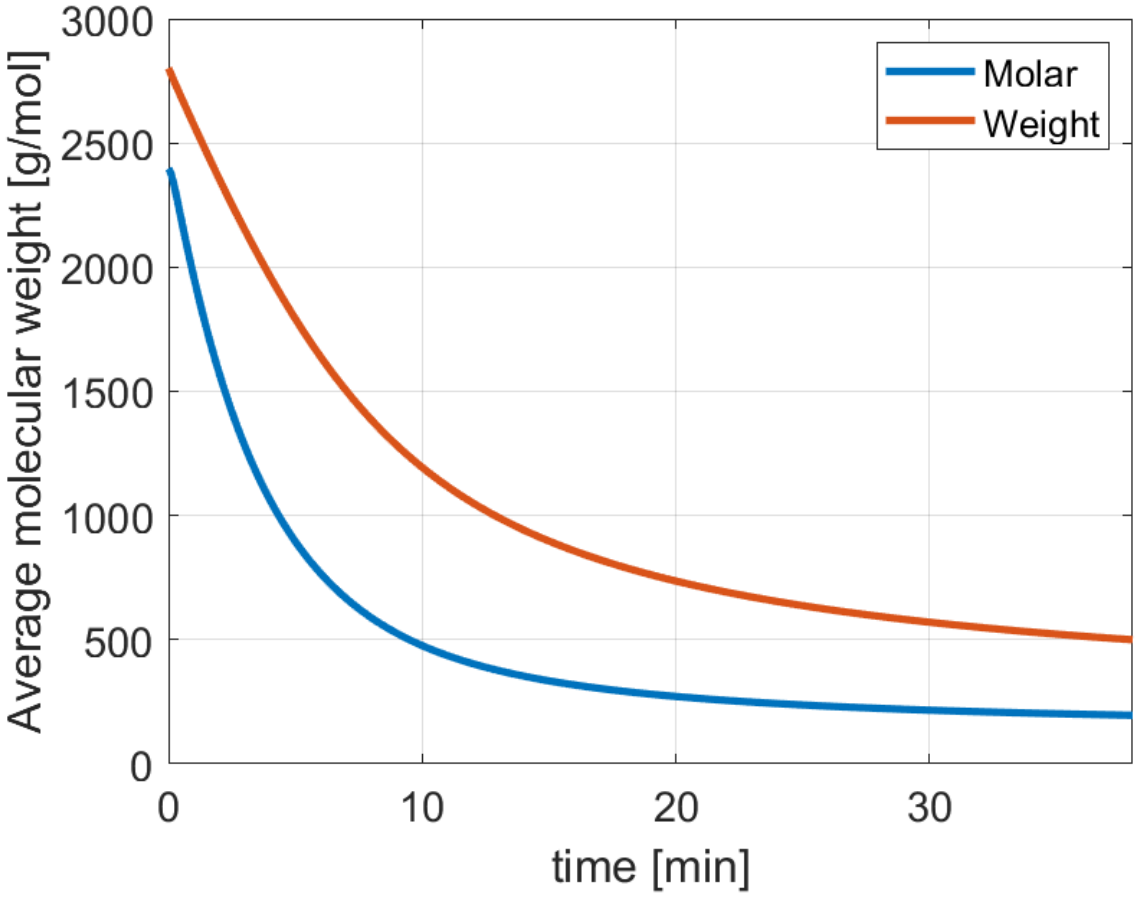

Figure C.12: Modelled total molecular weight for average mass and mole over time

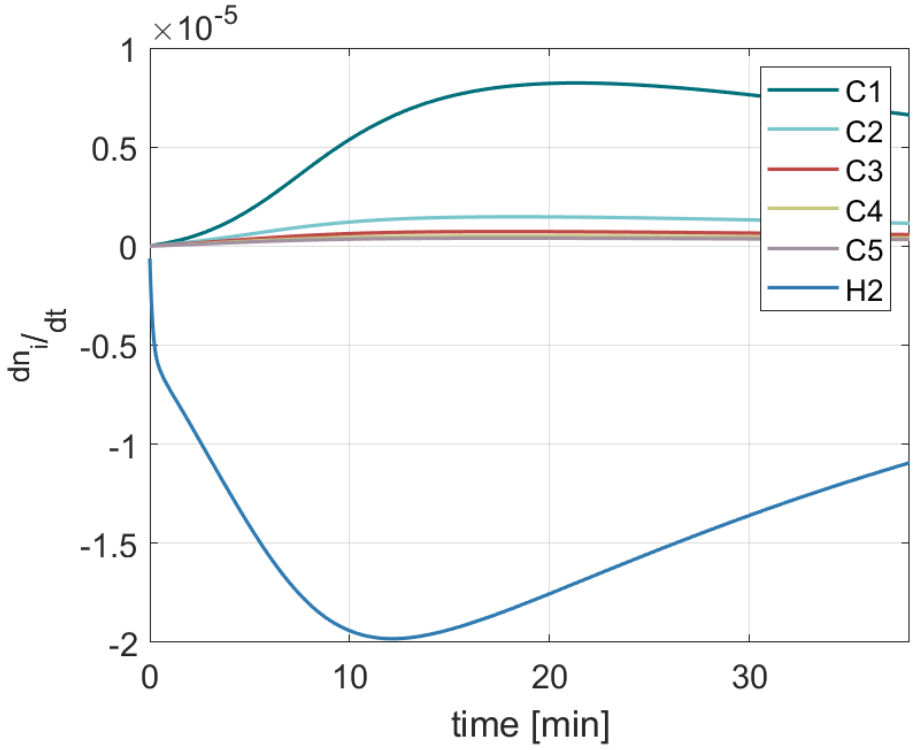

Figure C.13: Modelled evaporation rate for some compounds over time

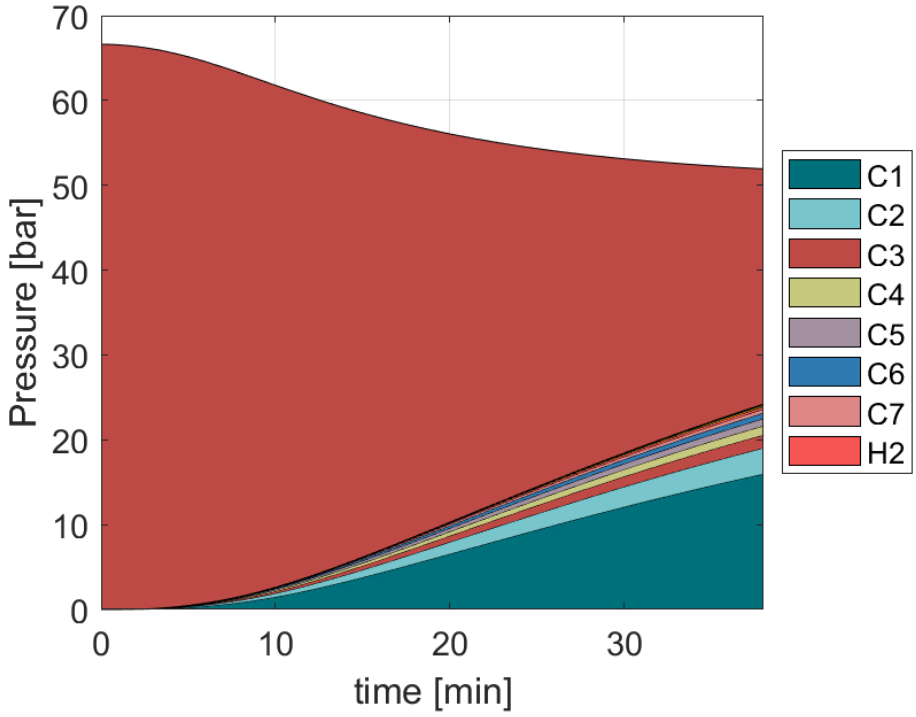

Figure C.14: Modelled pressure composition for evaporating compounds over time

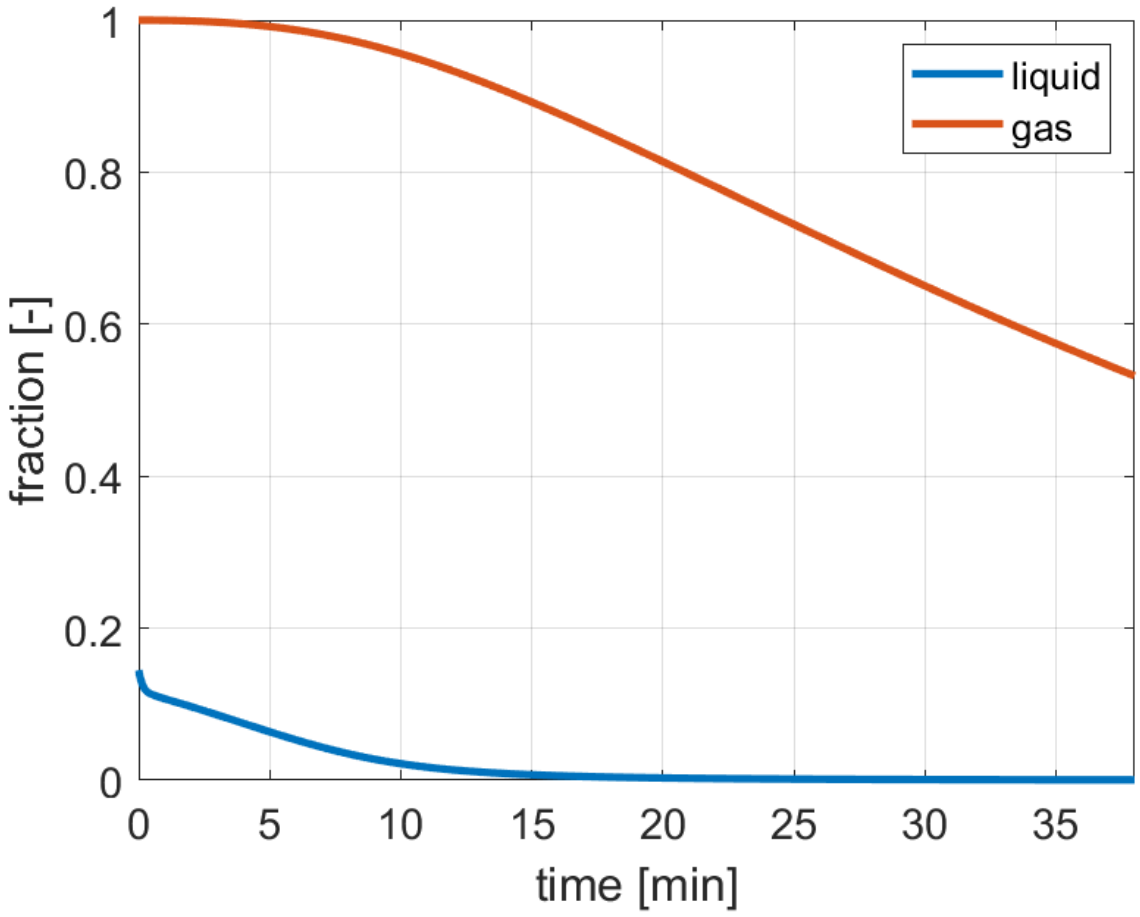

Figure C.15: Modelled hydrogen molar fraction in both phases over time

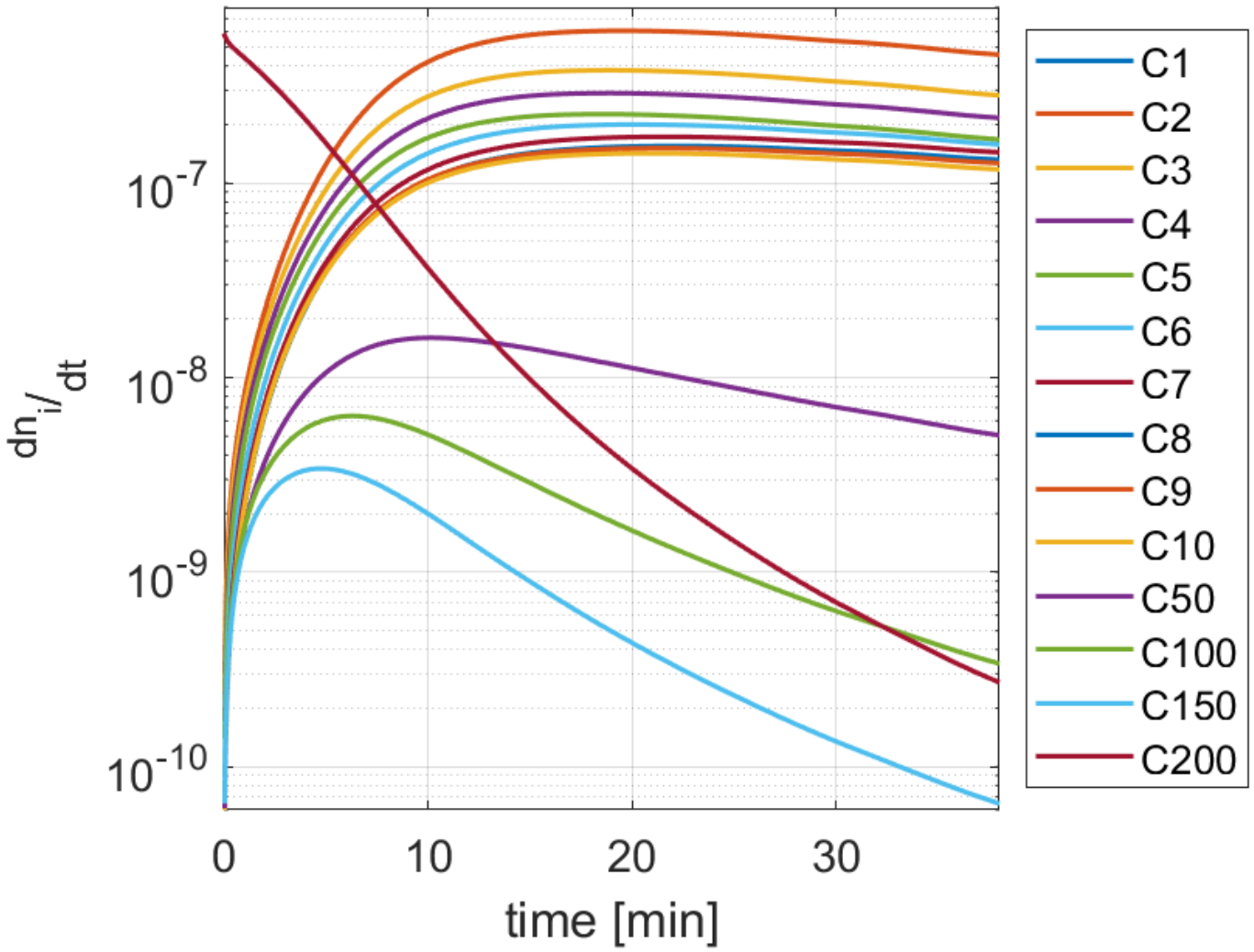

Figure C.16: Modelled hydrogenolysis rates of some hydrocarbons over time

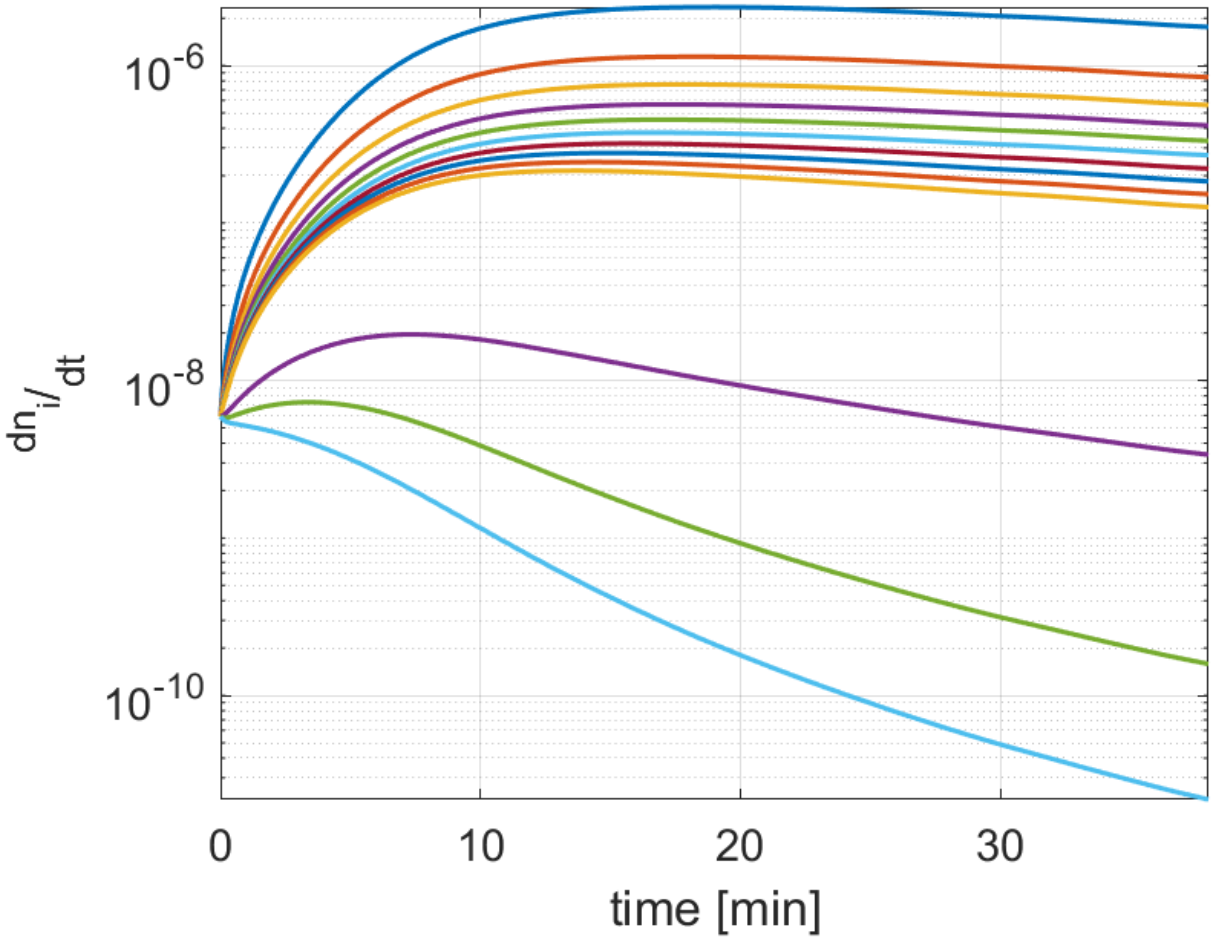

Figure C.17: Modelled formation rates of some hydrocarbons over time. See legend in figure C.16

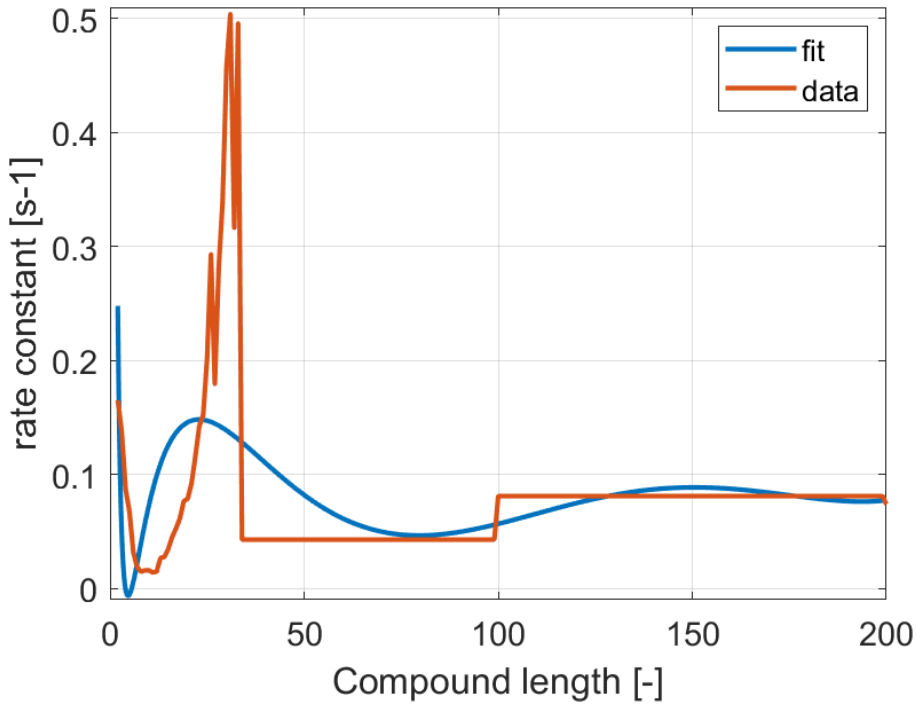

Figure C.18: Modelled kinetic reaction constants and the fitted description of them. See equation C.2 and the parameters in table C.2

Appendix D

Statistics

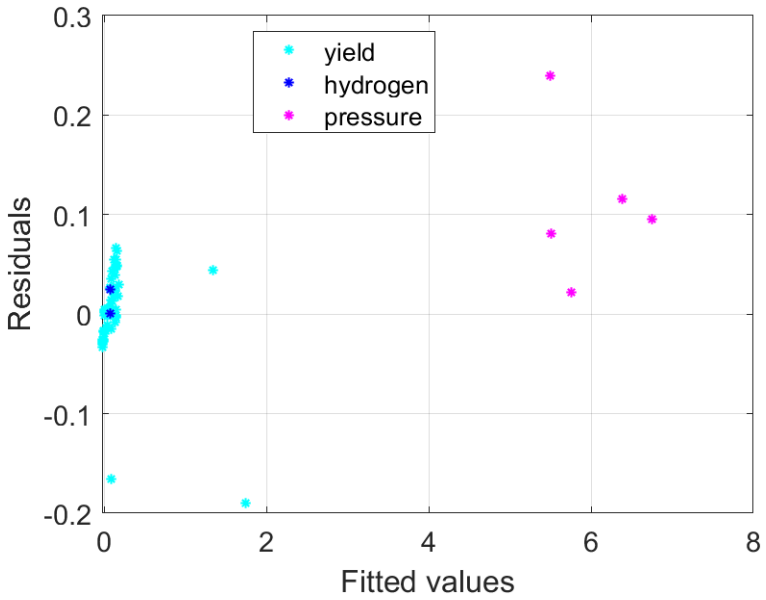

Figure D.1: Modelled residuals against modelled results

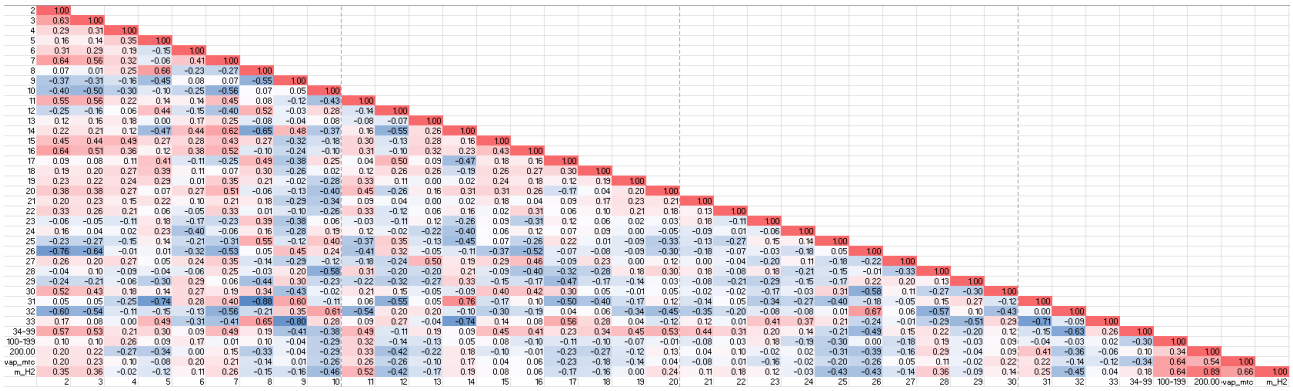

Figure D.2: Modelled correlation matrix for parameters